Department
of
APPLIED MATHEMATICS

Fresh Water driven primary Production in a Fjord

by

Jarle Berntsen, Dag L. Aksnes and Arne Foldvik

Report no. 107

March 1997

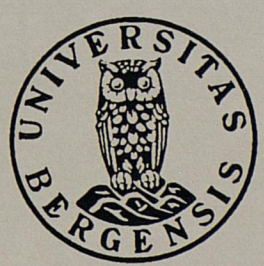

UNIVERSITY OF BERGEN
Bergen, Norway

Department of Mathematics
University of Bergen
5007 Bergen
Norway

ISSN 0084-778x

Fresh Water driven primary Production in a Fjord

by

Jarle Berntsen, Dag L. Aksnes and Arne Foldvik

Report No. 107

March 1997

Fresh water driven primary production in a fjord

Jarle Berntsen[1], Dag L. Aksnes[2] and Arne Foldvik[3]

Abstract. A coupled physical-chemical-biological ocean model has been applied to study the primary production in a fresh water driven idealized 60km long and 4km wide fjord without a sill. The model system is run for three different scenarios: a) Without fresh water runoff. b) A river at the bottom of the fjord adds $100m^3s^{-1}$ fresh water to the surface layer of the fjord. c) A river at the bottom of the fjord adds $90m^3s^{-1}$ fresh water to the surface layer and $10m^3s^{-1}$ is driven by potential energy from a dam near the river outlet through a pipe that enters the fjord at 50 depth. The average productions in the inner 45km of the fjord for the three scenarios are 80, 88 and 351 gCm^{-2} year^{-1} respectively. It is thus shown that there may be a considerable potential for increasing the primary production in many fjords and coastal areas by submerging some of the fresh water runoff from the rivers.

[1]Department of Mathematics, University of Bergen, Johs. Bruns gt 12, 5008 Bergen

[2]Department of Fisheries and Marine Biology, University of Bergen, Thormøhlens gt 55, 5008 Bergen

[3]Geophysical Institute , University of Bergen, Allegt. 17, 5007 Bergen

Contents

1 Introduction

It has been suggested to enhance the harvestable productivity of the marine system by fertilizing the surface layer of the ocean, and this is also the motivation behind the international research program, MARICULT [3]. At the University of Bergen and the Institute of Marine Research numerical models have been developed and used to study the response of marine systems to variations in nutrient supplies, see [1, 2, 5, 15, 17, 16]. In the MARICULT program description it is suggested that the least expensive fertilization method is the addition of formulated fertilizer to surface waters. An alternative will be to create upwelling of nutrient rich deep waters by submerging fresh water outlets from the surface to greater depths, see [9]. Due to buoyancy dived fresh water in a saline ocean will rise towards the surface and on the way the fresh water will mix with the ambient nutrient rich waters. By building a dam with surface level a few meters above the surface level of the fjord and leading a pipe from the bottom of the dam to for instance 50m depth in the fjord, the potential energy difference will be sufficient to drive the fresh water through the pipe. In the present study we have chosen to focus on the effects on the primary production of such a submerged fresh water outlet in an idealized fjord where the only driving forces are light, heating/cooling from the surface and fresh water.

2 The physical variables and equations

The physical variables and governing equations for these are given in Berntsen et al. [5]. For completeness these are repeated below. The symbols used in the description of the physical model are:

$\vec{U} = (U, V)$	Horizontal velocities in $x-$ and y-direction respectively
W	Vertical velocity in z-direction
η	Surface elevation
H	Bottom static depth
D	Bottom dynamic depth $(H + \eta)$
P	Pressure
ρ	Density
ρ_0	Reference density
S	Salinity
T	Temperature
K_M	Vertical eddy viscosity
A_M	Horizontal eddy viscosity
K_H	Vertical eddy diffusivity
A_H	Horizontal eddy diffusivity
g	Gravity
f	The Coriolis parameter
$\vec{U_b} = (U_b, V_b)$	Horizontal velocities at the bottom

The governing equations are:

$$\nabla \cdot \vec{U} + \frac{\partial W}{\partial z} = 0, \tag{1}$$

$$\frac{\partial U}{\partial t} + \vec{U} \cdot \nabla U + W\frac{\partial U}{\partial z} - fV = -\frac{1}{\rho_0}\frac{\partial P}{\partial x} + \frac{\partial}{\partial z}(K_M \frac{\partial U}{\partial z}) + F_x, \tag{2}$$

$$\frac{\partial V}{\partial t} + \vec{U} \cdot \nabla V + W\frac{\partial V}{\partial z} + fU = -\frac{1}{\rho_0}\frac{\partial P}{\partial y} + \frac{\partial}{\partial z}(K_M \frac{\partial V}{\partial z}) + F_y, \tag{3}$$

$$P = g\rho_0\eta + g\int_z^0 \rho(\acute{z})d\acute{z}, \tag{4}$$

The conservation equations for temperature and salinity are

$$\frac{\partial T}{\partial t} + \vec{U} \cdot \nabla T + W\frac{\partial T}{\partial z} = \frac{\partial}{\partial z}(K_H \frac{\partial T}{\partial z}), \tag{5}$$

$$\frac{\partial S}{\partial t} + \vec{U} \cdot \nabla S + W\frac{\partial S}{\partial z} = \frac{\partial}{\partial z}(K_H \frac{\partial S}{\partial z}). \tag{6}$$

In the present study we have regarded it to be sufficient to apply a simplified equation of state of the form

$$\rho = \rho(T, S) \tag{7}$$

taken from [19] instead of the UNESCO equation of state [18].

The horizontal viscous terms F_x and F_y are all written in the form:

$$F = \frac{\partial}{\partial x}(A\frac{\partial F}{\partial x}) + \frac{\partial}{\partial y}(A\frac{\partial F}{\partial y}). \tag{8}$$

The horizontal viscosity, A, is selected to be $100m^2s^{-1}$.

The vertical viscosity, K_M, and vertical diffusivity, K_H, are computed as functions of the Richardson number according to a formulation due to Munk and Anderson [11]

$$\begin{aligned} K_H &= 10^{-3}m^2s^{-1} \times (1 + 3.33Ri)^{-1.5} \\ K_M &= 10^{-3}m^2s^{-1} \times (1 + 10Ri)^{-0.5} \end{aligned}$$

where the Richardson number, Ri, is defined by

$$Ri = -\frac{\left(\frac{g}{\rho_0}\frac{\partial \rho}{\partial z}\right)}{\left(\left(\frac{\partial U}{\partial z}\right)^2 + \left(\frac{\partial V}{\partial z}\right)^2\right)}.$$

For $Ri \leq 0$, we choose $K_M = K_H = 0.05m^2s^{-1}$. Values of vertical viscosity and diffusivity for neutrally stable and unstable situations found in literature are typically of the same order of size as the value given above. The vertical viscosity and diffusivity terms of the governing equations are used to parameterize subgrid scale vertical mixing processes. It may be argued that in the case of submerged fresh water outlets the shape(s) and size(s) of the opening(s) may probably be tuned to create mixing vertically that correspond to the chosen value for K_M and K_H.

The Coriolis parameter is chosen to be: $f = 1.3 \times 10^{-4}s^{-1}$.

3 The chemical-biological variables and equations

The biological-chemical model has been used in a number of studies, see for instance [1, 2, 16]. For a complete description we refer to Skogen [15]. For completeness the governing equations, initial and boundary values for the biological-chemical variables nitrate, phosphate, silicate, detritus, flagellates, diatoms and also light in the water column are included below.

3.1 Light in the water column

Following Skartveit and Olseth [14] we let the suns declination, δ, as a function of day number, n, be given by

$$\sin\delta = 0.3979\sin(0.9856(n-80) + 1.9171[\sin(0.9856n) - 0.98112]). \tag{9}$$

Let SST be real sun time, CET Norwegian normal time and L the longitude. According to [14] SST is then given by

$$\begin{aligned} SST &= CET + (L-15) - 0.4083\sin[0.9856(n-80)] - \\ &\quad -1.7958\cos[0.9856(n-80)] + 2.4875\sin[1.9712(n-80)]. \end{aligned} \tag{10}$$

The sun elevation, h, may then be computed from

$$\sin h = \sin\delta\sin B - \cos\delta\cos B\cos(SST), \tag{11}$$

where B is the latitude. In our experiments we have chosen $L = 6.$ and $B = 60.$

The incident irradiation is modeled using a formulation of Skartveit and Olseth [13]. Their formulation give a *mean* irradiation as a function of latitude and season. This mean climatological irradiance, varies according to a presumed sinusoidal variation, and all constants, $a_x - f_x$, should be specific for the area to be modeled. The irradiance is split into a diffuse ($x = dif$) and a direct ($x = dir$), or beam, component

$$H_x(h,n) = I_0(n) \times Tr_{0x}(n) \times F_x(h). \tag{12}$$

Here $H_x(h,n)$ is either direct or diffuse irradiance at the surface, $I_0(n)$ the solar irradiance at normal incidence just outside the atmosphere, $Tr_{0x}(n)$ the transmittance and $F_x(h)$ the solar elevation function. Further h is the solar elevation and n the day number. The transmittance at overhead zenith sun is given by :

$$Tr_{0x}(n) = a_x(1 + b_x\cos\frac{n-c_x}{365}2\pi). \tag{13}$$

The solar elevation function, $F_x(h)$, expresses the effect of varying solar elevation, which is estimated in every internal time step, and is given by :

$$F_x(h) = 1 - d_x + e_x + d_x \sin h - e_x(\sin h)^{1/2}. \tag{14}$$

The formulas are valid when the solar elevation is above 5 degrees, nevertheless they are used for all solar elevations. Values of the parameters $a_x - e_x$ above are taken from Skartveit and Olseth [13] and are representative for a cloudless Bergen, see the table below.

a_{dir}	=	0.722	a_{dif}	=	0.094
b_{dir}	=	0.044	b_{dif}	=	0.052
c_{dir}	=	21	c_{dif}	=	64
d_{dir}	=	1.643	d_{dif}	=	-0.432
e_{dir}	=	-0.748	e_{dif}	=	1.718

Table 1. Parameters for direct and diffusive irradiance. (From Skartveit and Olseth [13])

The solar irradiance function, $I_0(n)$, is given by

$$I_0(n) = 1367.(1. + 0.03346 \cos[0.9856(n - 3)]). \tag{15}$$

Following the procedure above we may now approximate the incident direct and diffuse irradiation at the surface. In our model we need, however, the photosynthetic active irradiation at different depths of the water column.

The diffuse light is calculated from

$$I_{dif}(x, y, z, t) = PAR \times R_{dif}(x, y, t)\, e^{-\frac{\kappa(x,y,z,t)}{\mu}}, \tag{16}$$

where $R_{dif}(x, y, t) = H_{dif}(h, n)$, the diffuse component of the surface irradiance, and PAR, photosynthetic available radiance, a constant which converts from incident diffuse irradiation to photosynthetic active irradiation. μ is the mean cosine of the diffuse light (see [12]), and κ the attenuation coefficient which is kept as a function of the concentration of chlorophyll and "other substances".

$$\kappa = b_2\, z + \frac{\nu}{N2Chla} \int_z^0 (Dia(x, y, z, t) + Fla(x, y, z, t))dz. \tag{17}$$

Here ν is the chlorophyll-a light extinction coefficient, $N2Chla$ the fraction of nitrate and chlorophyll_a in a cell, b_2 extinction due to water and other substances, Dia the concentration of diatoms and Fla the concentration of flagellates.

A similar formulation to (16) is given for the direct light, $I_{dir}(x, y, z, t)$, by substituting R_{dif} with R_{dir} and μ with $\cos\phi$, where ϕ is the zenith angle of the direct light in the water column computed from Snells formula, $n_1 \cos h = n_2 \sin\phi$, where n_1 and n_2 are the refraction coefficients for air and water.

Symbol	Value/unit	Explanation
PAR	0.40	Photosynthetic active irradiance
μ	0.83	Mean cosine of diffuse light
b_2	$0.07m^{-1}$	Extinction due to water
$N2Chla$	11.0 mg N (mg Chl a)$^{-1}$	Cellular fraction of nitrate and Chl a
ν	$0.0138m$ (mg Chl a)$^{-1}$	Chl a light extinction coefficient
n_1	1.0	Refraction coefficient for air
n_2	1.34	Refraction coefficient for water

Table 2 Table of light parameters used in the above equations.

3.2 Primary production

Let the operator $\frac{D}{Dt}$ be defined by

$$\frac{D}{Dt} = \frac{\partial}{\partial t} + \vec{U}\cdot\nabla + W\frac{\partial}{\partial z} - \frac{\partial}{\partial z}(K_M\frac{\partial}{\partial z}) - \frac{\partial}{\partial x}(A_H\frac{\partial}{\partial x}) - \frac{\partial}{\partial y}(A_H\frac{\partial}{\partial y}).$$

Following [15] the chemical-biological variables may then be written

$$\begin{aligned}
\frac{DN}{Dt} &= R_{Dia} + R_{Fla} + c_4\,Det - (P_{Dia} + P_{Fla}) \\
\frac{DP}{Dt} &= c_1(R_{Dia} + R_{Fla} + c_4\,Det - (P_{Dia} + P_{Fla})) \\
\frac{DSi}{Dt} &= -c_2\,P_{Dia} \\
\frac{DDet}{Dt} &= c_3\,(Dia + Fla) - c_4\,Det \\
\frac{DDia}{Dt} &= P_{Dia} - R_{Dia} - c_3\,Dia \\
\frac{DFla}{Dt} &= P_{Fla} - R_{Fla} - c_3\,Fla
\end{aligned}$$

where the prognostic variables are

N	Inorganic nitrogen,
P	Inorganic phosphate,
Si	Inorganic silicate,
Det	Detritus,
Dia	Diatoms and
Fla	Flagellates ,

and where the terms on the right hand side are sink/source terms to be specified, P production terms, R metabolic loss terms, c_1 intercellular P/N relationship, c_2 intercellular Si/N relationship, c_3 phytoplankton death rate and c_4 regeneration rate of detritus.

The metabolic losses for diatoms are assumed to be related to the temperature according to the equation

$$R_{dia}(x,y,z,t) = a_5\, Dia(x,y,z,t)\, e^{a_6 T(x,y,z,t)}, \tag{18}$$

with a_5 and a_6 the metabolic loss rate at $0\,^{\circ}C$ (s^{-1}) and the metabolic loss rate temperature dependence $(^{\circ}C^{-1})$ respectively. For flagellates the corresponding equation is

$$R_{fla}(x,y,z,t) = a_5\, Fla(x,y,z,t)\, e^{a_6 T(x,y,z,t)}. \tag{19}$$

The death rate of the algae (in the whole water column) is assumed to be constant as long as the chlorophyll concentration of the algae at the surface is above a minimum level, and zero if it is below. This is because the biological model is light limited in winter, and in order to prevent the algae in the model to extinct, further death when their concentration becomes too small, must be prevented.

Let μ_{dmax} be the specific growth rate of the diatom population under optimum light and nutrient conditions. The growth rate is made temperature dependent as suggested in [8]. The relation

$$\mu_{dmax}(x,y,z,t) = a_1 e^{a_2 T(x,y,z,t)}, \tag{20}$$

is chosen, where a_1 is the diatom production maximum at $0\,^{\circ}C$ (s^{-1}), and a_2 is the production rate temperature dependence $(^{\circ}C^{-1})$ for diatoms. For flagellates the corresponding expression becomes

$$\mu_{fmax}(x,y,z,t) = a_3 e^{a_4 T(x,y,z,t)}. \tag{21}$$

The relationship between phytoplankton production and light intensity, and the relationship between phytoplankton production and nutrient uptake is represented

by an affinity formulation, see [16]. The combined effects of nutrient and light limitation are multiplicative and given by :

$$P_{dia}(x,y,z,t) = \mu_{dmax} \times V_{d1} \times N_{dlim} \times Dia(x,y,z,t), N_{dlim} = \min_{2 \le i \le 4} V_{di}, \quad (22)$$

where

$$V_{di} = \frac{S_{di}}{S_{di} + \frac{\mu_{dmax}(T)}{\alpha_{di}}}, \; i = 1, \ldots, 4 \quad (23)$$

is a modified Michaelis-Menten limitation for substance S_{di}. In the equations $i = 1$ corresponds to the sum of direct and diffuse irradiance, $i = 2$ to nitrate, $i = 3$ to phosphate and $i = 4$ to silicate. Analogous formulations are used for the production of flagellates. The only difference is that silicate is non-limiting for flagellates.

Diatoms, flagellates and detritus are allowed to sink with velocities s_{dia}, s_{fla} and s_{det}. For diatoms the rate is made silicate dependent and varies between s_{diamin} and s_{diamax}. The values of the above parameters are given in [2] and [16] and repeated in Table 3.

Symbol	Value/unit	Explanation
a_1	$1.53 \times 10^{-5} s^{-1}$	Maximum growth rate for diatoms at $0\,^{\circ}C$
a_2	$0.063 ^{\circ}C^{-1}$	Temperature dependency of growth for diatoms
a_3	$1.02 \times 10^{-5} s^{-1}$	Maximum growth rate for flagellates at $0\,^{\circ}C$
a_4	$0.063 ^{\circ}C^{-1}$	Temperature dependency of growth for flagellates
a_5	$8.05 \times 10^{-7} s^{-1}$	Metabolic loss rate at $0^{\circ}C$
a_6	$0.07 ^{\circ}C^{-1}$	Metabolic loss rate temperature dependence
c_1	0.138 mg P (mg N)$^{-1}$	Intercellular P/N relationship
c_2	1.75 mg Si (mg N)$^{-1}$	Intercellular Si/N relationship
c_3	$1.6 \times 10^{-6} s^{-1}$	Death rate of phytoplankton
c_4	$1.52 \times 10^{-7} s^{-1}$	Decomposition rate detritus
α_{d1}	$3.6 \times 10^{-7} m^2 \mu\text{Einstein}^{-1}$	Growth affinity for irradiance for diatoms
α_{f1}	$1.1 \times 10^{-7} m^2 \mu\text{Einstein}^{-1}$	Growth affinity for irradiance for flagellates
α_{d2}	$1.7 \times 10^{-5} s^{-1} \mu M^{-1}$	Growth affinity for nitrate for diatoms
α_{f2}	$1.5 \times 10^{-5} s^{-1} \mu M^{-1}$	Growth affinity for nitrate for flagellates
α_{d3}	$2.7 \times 10^{-4} s^{-1} \mu M^{-1}$	Growth affinity for phosphate for diatoms
α_{f3}	$2.5 \times 10^{-4} s^{-1} \mu M^{-1}$	Growth affinity for phosphate for flagellates
α_{d4}	$2.5 \times 10^{-5} s^{-1} \mu M^{-1}$	Growth affinity for silicate for diatoms
s_{diamax}	$3m$ day^{-1}	Maximum sinking rate diatoms
s_{diamin}	$0.3m$ day^{-1}	Minimum sinking rate diatoms
s_{fla}	$0.25m$ day^{-1}	Sinking rate flagellates
s_{det}	$3m$ day^{-1}	Sinking rate detritus

Table 3 Values for the parameters of the phytoplankton model.

4 The numerical experiment

The model domain described in Figure 1 is $0 \leq x \leq L_x$, $0 \leq y \leq L_y$ with $L_x = 60000$m and $L_y = 4000$m. There are vertical walls at $y = 0$ and $y = L_y$. There is also a vertical wall at $x = 0$ except for a river outlet to be specified. At $x = L_x$ there is an open boundary to the coast. The bottom depth, $H(x, y)$, is equal to 250m for all x and y.

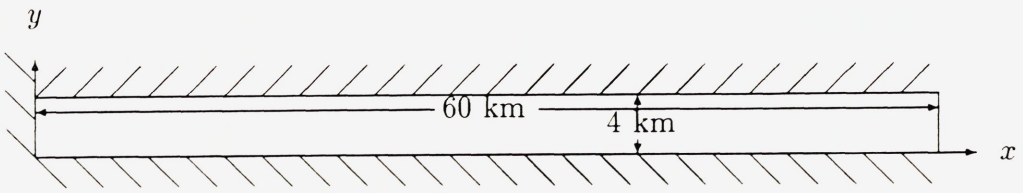

Figure 1 The computational domain.

A three dimensional σ-coordinate circulation model, see Berntsen et al. [5], is used to approximate the prognostic physical variables and also to advect the prognostic chemical-biological variables with the computed currents. Routines for light and sink and source terms for the chemical and biological variables are taken from NORWECOM [15].

Horizontally the spatial resolution is 1km in both directions. Vertically 51 σ-coordinate layers are used. The layers are chosen to give high resolution near the surface. When the surface elevation is zero, the 6 layers near the surface are 0.5m thick. The following layers are 0.75m, 1.0m, 1.25m, 1.5m and 1.75m thick. From 9.25m depth down to 49.25m the layers are 2.0m thick. From 49.25m the layers are 2.25m, 2.5m, 3.0m, 3.5m, 4.0m, 4.5m, 5.0m, 5.5m, 6.0m, 7.0m, 8.0m, 9.5m, 11.5m, 13.0m, 14.5m, 16.0m, 17.5m, 20.0m, 22.5m and 25.0m thick.

The model is run for different scenarios over a model year starting 1/1 and ending 31/12. The model time step is chosen to be 120s.

The circulation and biological processes in the fjord are to a great extent determined by the boundary values for all prognostic variables and also the initial values. In particular the processes are influenced by riverine inputs to the system and the choice of boundary conditions at the open boundary $x = L_x$. The solutions are sensitive to the choice of boundary conditions. Below the choices made in this study are described. Other methods for introducing fresh water into the fjord and for treating the open boundary have been tried. Here we focus on the experiments that have given, so far, model currents in 'best' qualitative agreement with the expected circulation.

4.1 Initial and boundary values

4.1.1 Velocities and the water elevation

Initially $U = V = W = 0ms^{-1}$ and $\eta = 0m$. At the outflow a 10-grid cell wide FRS-zone is used, see Martinsen and Engedahl [10]. Each prognostic variable, ϕ, in the zone is after each model time step updated according to

$$\phi = (1-\alpha)\phi_{int} + \alpha\phi_{ext},$$

where ϕ_{int} contains the unrelaxed values computed by the model and ϕ_{ext} is a specified external solution in the zone. The relaxation parameter α varies from 1 at $x = L_x$ to 0 at the end of the zone facing the interior model domain. The quality of this flow relaxation scheme depends strongly upon the quality of the specified external solutions, ϕ_{ext}, chosen for the prognostic variables.

For η we apply $\eta_{ext} = 0$m as the specified external solution. v_{ext} is chosen to be $0ms^{-1}$. Approximations to the integral

$$\frac{1}{10000}\int_{x=35000m}^{x=45000m} u(x,y,z)dx$$

are computed for each time step from approximations to $u(x,y,z)$ in the interior model domain and applied as the external boundary values for u. This choice of u_{ext} allows the average interior velocity profile to propagate through the open boundary.

At the free surface no wind stress

$$K_M\frac{\partial\vec{U}}{\partial z} = 0, \qquad z = \eta$$

is assumed. A quadratic law for the bottom stress

$$K_M\frac{\partial\vec{U}}{\partial z} = c_d(U_b^2 + V_b^2)^{1/2}\vec{U}_b, \qquad z = H(x,y),$$

where

$$c_d = \max[0.0025, \frac{\kappa^2}{(ln(z_b/z_0))^2}]$$

and z_b is the distance of the nearest grid point to the bottom, is applied. The von Karman constant $\kappa = 0.4$. The bottom roughness parameter $z_0 = 0.01m$.

For the closed horizontal boundaries no normal flux is assumed.

4.1.2 Salinity

On inflow the salinity at the open boundary is specified as a linear combination between the winter profile

$$S_1(z) = 0.5 \times (S_{max} + S_{minw}) - \Delta S_1 \times tanh\left(\frac{z - Z_s}{\Delta Z_s}\right),$$

and a typical summer stratified profile

$$S_2(z) = 0.5 \times (S_{max} + S_{mins}) - \Delta S_2 \times tanh\left(\frac{z - Z_s}{\Delta Z_s}\right),$$

where S_{max} = 35.0 p.s.u, S_{minw} = 32.0 p.s.u, S_{mins} = 25.0 p.s.u, ΔS_1 = (S_{max} - S_{minw})/2, ΔS_2 = (S_{max} - S_{mins})/2, $Z_s = -10m$ and $\Delta Z_s = 5m$. We assume a sinusoidal variation over the year and define

$$Frac(t) = 0.5 + 0.5 \times cos(2\pi(t - 30)/360), \tag{24}$$

where t is the time in days since the start of a new model year. The salinity at the outlet of the fjord is then specified according to

$$S(L_x, y, z, t) = Frac(t) \times S_1(z) + (1 - Frac(t)) \times S_2(z) \qquad \forall y. \tag{25}$$

On inflow ($u_{ext} < 0$) we have chosen $S_{ext}(y, z, t) = S(L_x, y, z, t)$. On outflow ($u_{ext} > 0$) a spatial average of the interior salinity field from $x = 35000m$ to $x = 45000m$, computed with the same technique as for u_{ext}, is used as S_{ext}. This allows coastal water masses to enter the fjord on inflow and interior water masses to leave the fjord on outflow. We compute external solutions for temperature and for the chemical-biological variables with the same technique.

As initial values we apply

$$S(x, y, z, 0) = S(L_x, y, z, 0) \qquad \forall x, y.$$

No precipitation or evaporation is assumed.

4.1.3 Temperature

The initial and boundary conditions for temperature are given by either an assumed fjord profile $T_{fjord}(z, t)$ or an assumed coastal profile $T_{coast}(z, t)$. Let a typical winter value of temperature in a fjord be

$$T_1(z) = 0.5 \times (T_{min} + T_{aver}) - \Delta T_1 \times tanh\left(\frac{z - Z_t}{\Delta Z_t}\right),$$

and a typical summer stratified profile be

$$T_2(z) = 0.5 \times (T_{max} + T_{aver}) + \Delta T_2 \times tanh\left(\frac{z - Z_t}{\Delta Z_t}\right),$$

where $T_{max} = 18.0$, $T_{min} = 0.0$, $T_{aver} = 8.0$, $\Delta T_1 = (T_{aver}$ - $T_{min})/2$, $\Delta T_2 = (T_{max}$ - $T_{aver})/2$, $Z_t = -10m$ and $\Delta Z_t = 5m$. Let $Frac(t)$ be given by (24). The fjord profile is then given by

$$T_{fjord}(z,t) = Frac(t) \times T_1(z) + (1 - Frac(t)) \times T_2(z)$$

To compute $T_{coast}(z,t)$ we apply the same formula with $T_{max} = 16.0$, $T_{min} = 4.0$, $T_{aver} = 10.0$, $Z_t = -20m$ and $\Delta Z_t = 10m$.

As initial values we apply

$$T(x,y,z,0) = T_{fjord}(z,0) \qquad \forall x,y.$$

In lack of information on surface heat fluxes, we relax the sea surface temperature towards typical fjord surface temperatures, see Cox and Bryan [7]. The surface flux of heat is specified by

$$K_H \frac{\partial T(x,y,0,t)}{\partial z} = \gamma(T_{fjord}(0,t) - T(x,y,0,t))$$

where K_H is the vertical diffusivity in the top layer and γ a time constant selected to be $1.735 * 10^{-5} ms^{-1}$. This means that during weak forcing the temperature in the upper 15m or so of the surface layer obtain the fjord surface value on a time scale of 10 days.

On inflow $T_{ext}(y,z,t) = T_{coast}(z,t)$ is used as a external boundary condition for all y.

4.1.4 The chemical and biological variables

External boundary values for inorganic nitrogen, phosphate and silicate at the open boundary are on inflow specified as a linear combination between winter unstratified profiles

$$\begin{aligned} N_1(z) &= N_{max}, \\ P_1(z) &= P_{max}, \\ Si_1(z) &= Si_{max}, \end{aligned}$$

and typical summer stratified profiles

$$
\begin{aligned}
N_2(z) &= 0.5 \times (N_{max} + N_{min}) - \Delta N \times tanh\left(\frac{z - Z_n}{\Delta Z_n}\right), \\
P_2(z) &= 0.5 \times (P_{max} + P_{min}) - \Delta P \times tanh\left(\frac{z - Z_n}{\Delta Z_n}\right), \\
Si_2(z) &= 0.5 \times (Si_{max} + Si_{min}) - \Delta Si \times tanh\left(\frac{z - Z_n}{\Delta Z_n}\right).
\end{aligned}
$$

A sinusoidal variation over the year for these variables is achieved by using the interpolation technique given by equations (24) and (25). As initial values we apply

$$
\begin{aligned}
N(x, y, z, 0) &= N(L_x, y, z, 0) \\
P(x, y, z, 0) &= P(L_x, y, z, 0) \\
Si(x, y, z, 0) &= Si(L_x, y, z, 0)
\end{aligned}
$$

For diatoms and flagellates the initial values are Dia_{min} and Fla_{min} respectively and these values are on inflow also used as external boundary values. On inflow during the summer these boundary values for diatoms and flagellates are probably too small. However, in studies where the focus is on new production in the fjord, we want to keep the imported biomass at a minimum level. Detritus is initialized to be zero and we also assume zero concentration of detritus through the open boundary on inflow. The table below gives the parameter values.

Symbol	Value/unit	Explanation
N_{max}	$15.0\mu M$	Maximum value of inorganic nitrogen
N_{min}	$0.0\mu M$	Minimum value of inorganic nitrogen
P_{max}	$1.0\mu M$	Maximum value of inorganic phosphate
P_{min}	$0.0\mu M$	Minimum value of inorganic phosphate
Si_{max}	$10.0\mu M$	Maximum value of inorganic silicate
Si_{min}	$0.0\mu M$	Minimum value of inorganic silicate
ΔN	$0.5 \times (N_{max} - N_{min})$	
ΔP	$0.5 \times (P_{max} - P_{min})$	
ΔSi	$0.5 \times (Si_{max} - Si_{min})$	
Z_n	$40m$	Depth of nutricline
ΔZ_n	$20m$	Thickness of nutricline
Dia_{min}	$2.75mgNm^{-3}$	Minimum value of diatoms
Fla_{min}	$2.75mgNm^{-3}$	Minimum value of flagellates

Table 4. Parameters of nutrient boundary value parameters.

4.2 Riverine inputs

At $x = 0$ and $y = L_y$ a river enters the fjord. The temperature of the freshwater follows the yearly cycle of the surface water of the fjord ($T_{fjord}(0,t)$). The concentrations of the nutrients (and of algaes) are chosen to be zero in the added fresh water. There are various ways of introducing fresh water runoffs into ocean/fjord models. In earlier experiments, see [4, 6, 16], for larger areas and with coarser grids, the added river water is added on top of the ocean water in the nearest coastal cell according to specified fresh water fluxes and then mixed with the oceanic water masses down to specified depths. For the present fjord study we have found that by taking the fresh water fluxes directly into all advective parts of the code in the nearest ocean cell, we are able to maintain a thin fresh water surface layer throughout the fjord. This is in qualitative agreement with observations.

The model has been run for three scenarios:

a) No fresh water flux. For this case there will be no currents and the primary production will be light, nutrient and temperature driven.

b) Fresh water with constant flux equal to $100m^3s^{-1}$ is added to the model domain into the upper 4 layers (2m depth) of the nearest coastal cell.

c) The same fresh water flux as under b) is applied, but now only $90m^3s^{-1}$ is added to the model domain into the upper 4 layers. We assume that the remaining $10m^3s^{-1}$ is led through a pipe down to 50m depth into the nearest fjord cell.

The input of fresh water far below the surface as in scenario c) above deserves some comments. The introduced fresh water will be subject to strong buoyant forces and will rise towards the surface. On the way towards the surface the ambient water masses will be mixed with the fresh water. The extent of this mixing for a real submerged fresh water outlet is unclear and will certainly depend on how the water is released. One could choose one wide opening of the pipe, many narrower ones and the angle of the pipe at the outlet(s) point(s) may be varied. The mixing will also depend on small scale processes near and above the outlet. In our coarse grid size hydrostatic model we can not represent the small scale processes and we let the vertical eddy viscosity/diffusivity take care of the vertical mixing. For unstable stratification, that is $\frac{\partial \rho}{\partial z} > 0$ or $Ri < 0$, which we typically will find above the outlet we have chosen $K_M = K_H = 0.05m^2s^{-1}$. With this representation the fresh water gets well mixed with the ambient water masses on its way towards the surface. Also the nutrients in the ambient deeper water masses are transported towards the surface. This increases clearly the potential for primary production.

5 Model results

5.1 Circulation and hydrography

The amount of data produced by the model is overwhelming and below a few instantaneous pictures of the current fields and salinity fields for scenarios b) and c) and two time series are presented. In figures 2a to 2d the along fjord currents after 5 days and after 100 days at $y = 500$m in the upper 50m are shown. The maximum velocity after 5 days is for both cases approximately $0.30ms^{-1}$. The maximum velocity after 100 days is for both cases approximately $0.064ms^{-1}$. In figures 3a and 3b the velocities normal to a cross section of the fjord at $x = 40000$m are given. The positive velocities (out of the fjord) are contoured with solid lines. The negative velocities are dotted. The instantaneous fields after 100 days for the two scenarios b) and c) are given respectively. The kinetic energies in Joule per m^3 for the whole year averaged over the whole fjord for cases b) and c) are given in Figure 4. The average transports out of the fjord over the last 11 months of the year are for scenario b) $302m^3s^{-1}$ when we integrate vertically over the upper 10m and $610m^3s^{-1}$ when we integrate over the upper 50m. For scenario c) the corresponding number is $2728m^3s^{-1}$ when we integrate over the upper 50m.

In figures 5a to 5b the along fjord salinity fields corresponding to the currents shown in Figure 2 are given. In figures 6a and 6b the cross fjord salinity fields corresponding to the normal velocities given in Figure 3 are plotted. The contour plots of salinity tend to smooth the salinity fields too much because of the interpolations involved, and time series of salinity taken in position $(x, y, z) = (30000\text{m}, 1000\text{m}, 0.5\text{m})$ give a better impression of the surface salinities, see Figure 7.

From figures 2 and 4 we note that there is much higher velocities and more kinetic energy in the spin up phase of the model than in the period after the first month. When fresh water initially is introduced into the fjord, there will be an increase in potential energy connected to higher horizontal gradients in salinity and density, see figures 5a and 5c. This will produce higher velocities in the system. After approximately 14 days the salinity and density fields of the fjord will be in more equilibrium with the supply of fresh water and we find much smaller horizontal density and salinity gradients, see figures 5b and 5d. Thus the source for production of kinetic energy will be much smaller after the initial spin up period. The stronger currents in the transient phase will also cause more vertical exchange of water masses and thus bring up nutrient rich waters to the surface. Therefore, by letting fresh water enter a fjord in pulses, there will be a potential for increased primary production.

By comparing the figures 2b, 3a, 5b and 6a with the corresponding sequence for the submerged case, we notice the effects of the submerged fresh water supply. In the steady state solution for scenario b) we have a thin layer (2-3m) of outflowing water masses above a layer (approximately 5m deep) of inflowing water. The outflowing

layer for scenario c) is much thicker. For this case the return flow typically occurs at depths greater than 50m and therefore the inflowing water will be very rich in nutrients. In scenario b) we have much less entrainment. From the average transports and simple budget considerations for volume and salinity it may be estimated that the average salinity of the outflowing water masses in scenario b) is 20 p.s.u. and 34.0 p.s.u. for scenario c). This is in qualitative agreement with the fields shown in Figure 6.

From Figure 7 we notice that towards the summer the salinity of the top layer of the model tends to decrease. This is due to increased stratification due to heating of the surface layer. Towards the winter we note an increase in salinity connected to the cooling and destratification of the surface.

The external Rossby radius for our fjord is approximately 10 times the width of the fjord. The radius of the first internal mode is more difficult to estimate, but will be of the same order of size as the width of the fjord (4000m). Some effects of the earths rotation are seen in the cross fjord velocity profiles of Figure 4 and also in the 34.9 p.s.u. contour in Figure 6b. The effects on depth integrated primary production is seen in figures 20a and 20b.

Figure 2a.

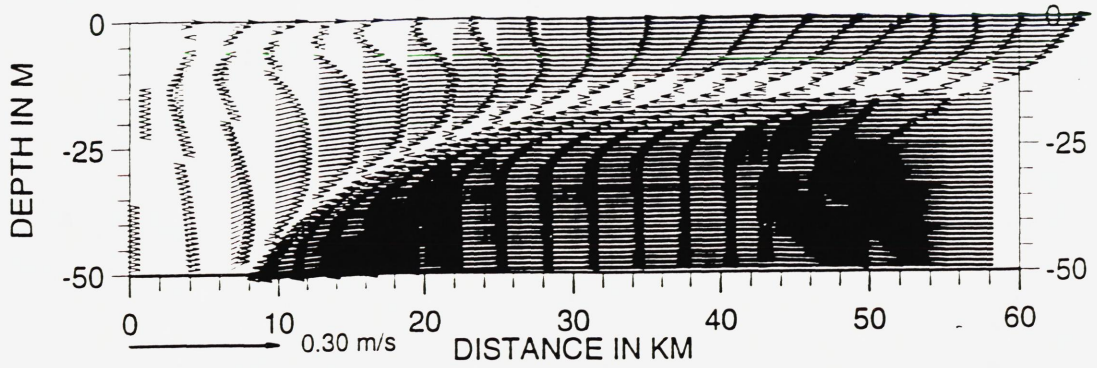

Figure 2b.

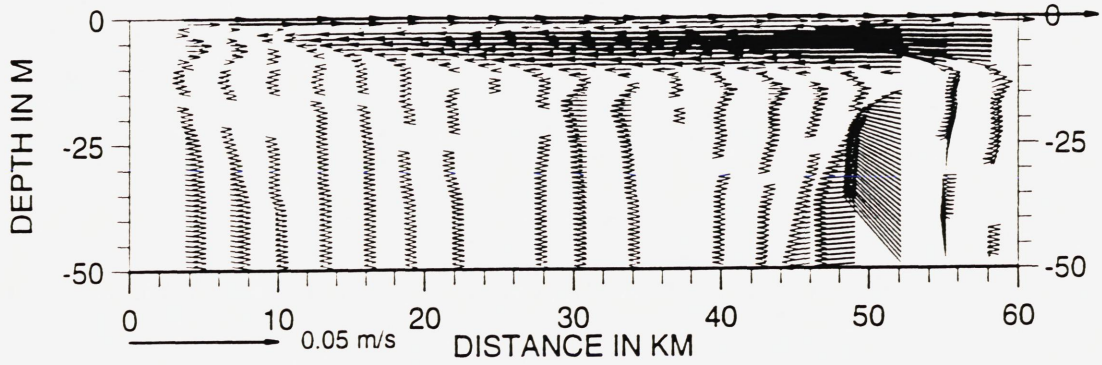

Figure 2c.

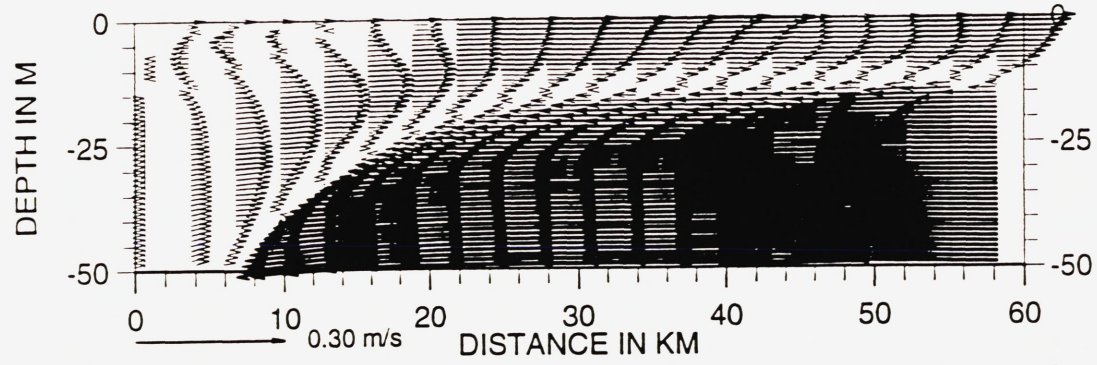

Figure 2d.

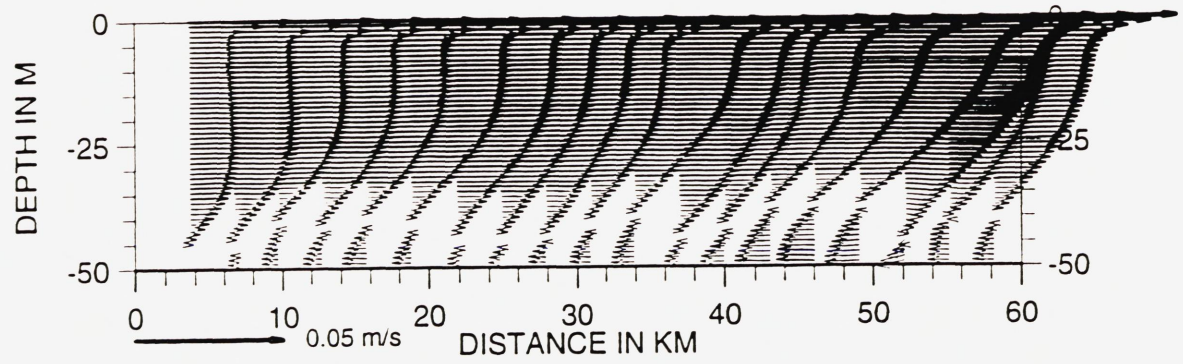

Figure 2. Along fjord currents in the upper 50m of the fjord at $y = 500$m. The velocities at the head of the displayed arrows indicate the scaling of the arrows in the fjord for each figure. All vertical components are multiplied by 100. Figure 2a: Scenario b) after 5 days. Figure 2b: Scenario b) after 100 days. Figure 2c: Scenario c) after 5 days. Figure 2d: Scenario c) after 100 days.

Figure 3a.

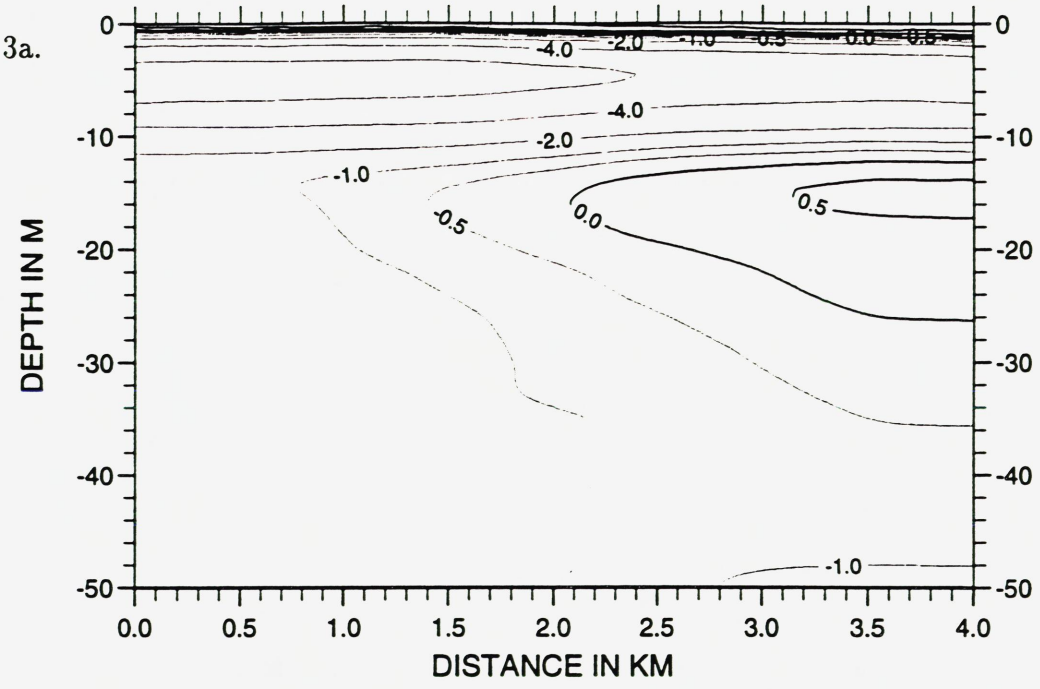

Figure 3b.

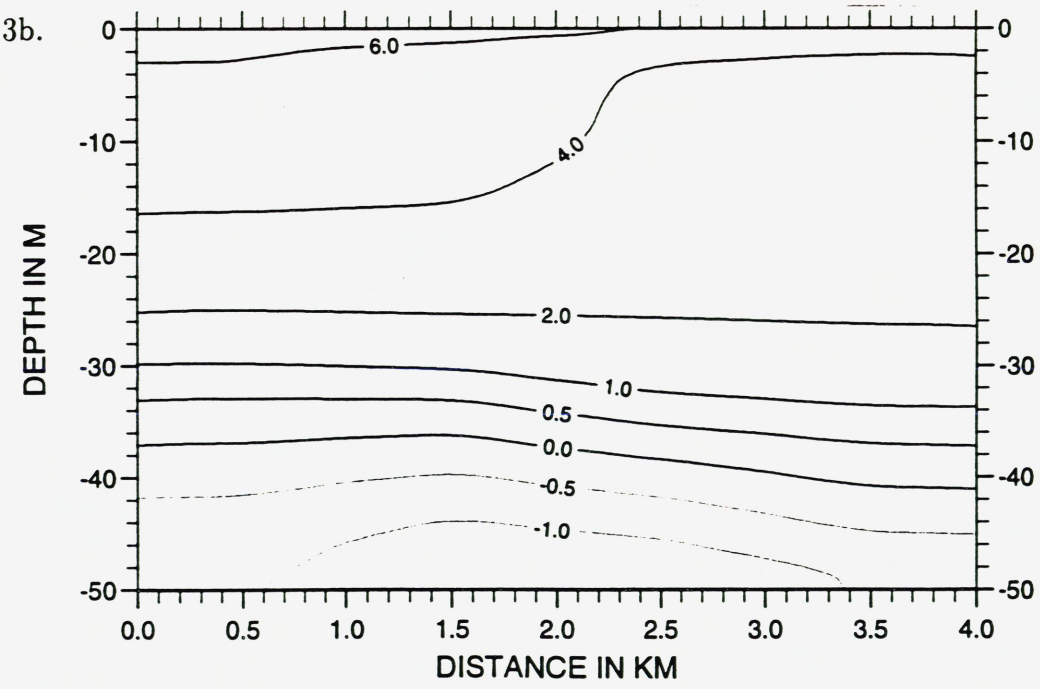

Figure 3. Cross fjord velocities in the upper 50m normal to a section at $x = 40000$m after 100 days. Outgoing velocities are indicated by solid lines. Dotted lines indicate flow into the fjord. Figure 3a: Scenario b). Figure 3b: Scenario c).

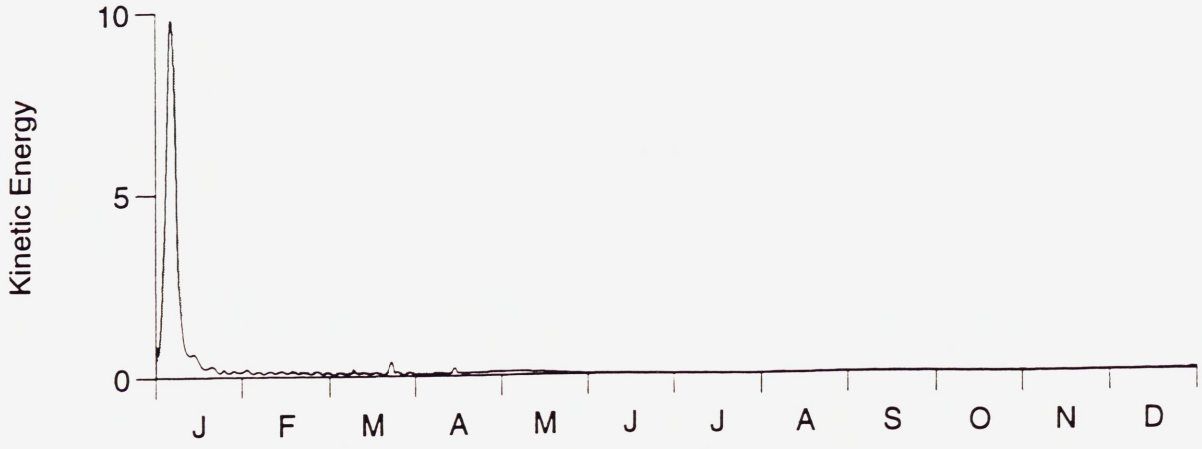

Figure 4. Kinetic energy averaged over the whole fjord in Joule per m^3 for scenario b) (solid line) and scenario c) (dotted line).

Figure 5a.

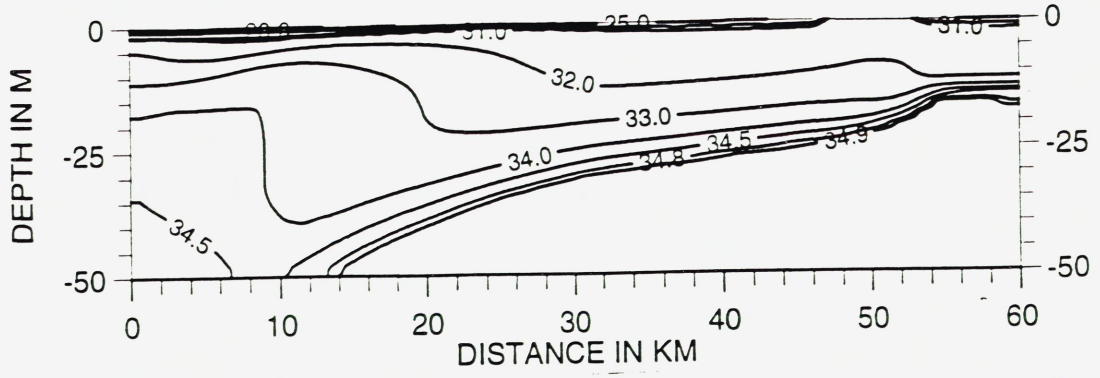

Figure 5b.

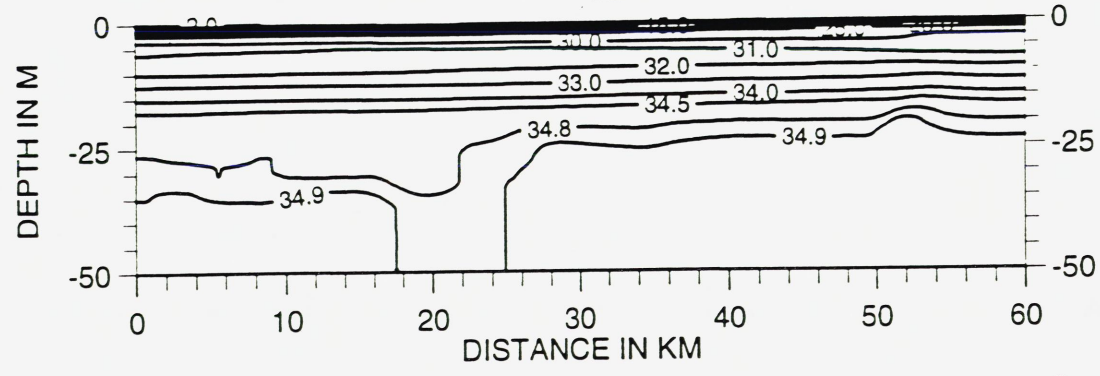

Figure 5c.

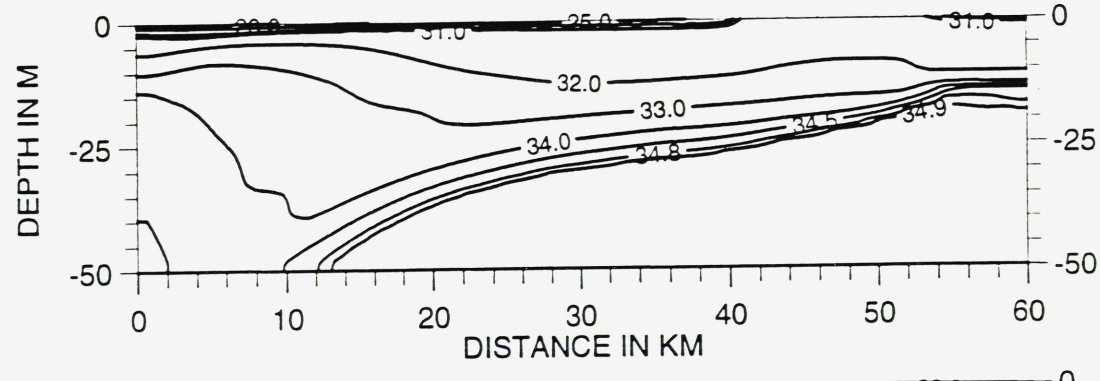

Figure 5d.

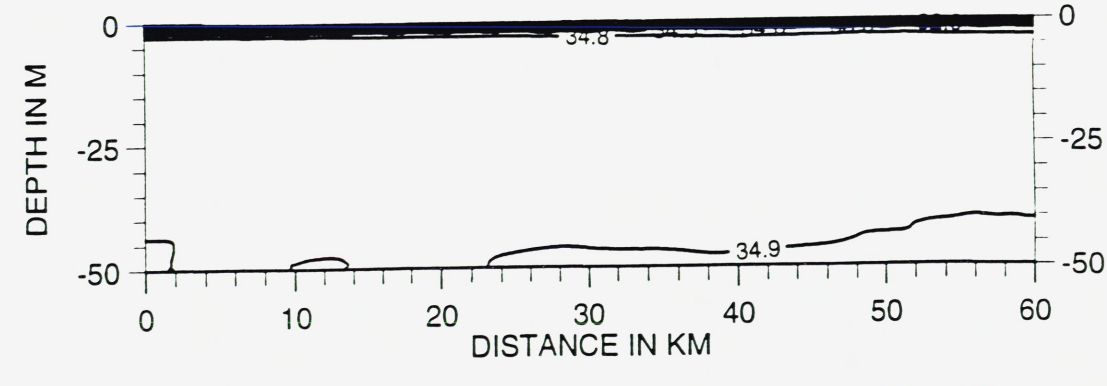

Figure 5. Along fjord salinities in the upper 50m of the fjord at $y = 500$m. Figure 5a: Scenario b) after 5 days. Figure 5b: Scenario b) after 100 days. Figure 5c: Scenario c) after 5 days. Figure 5d: Scenario c) after 100 days.

Figure 6a.

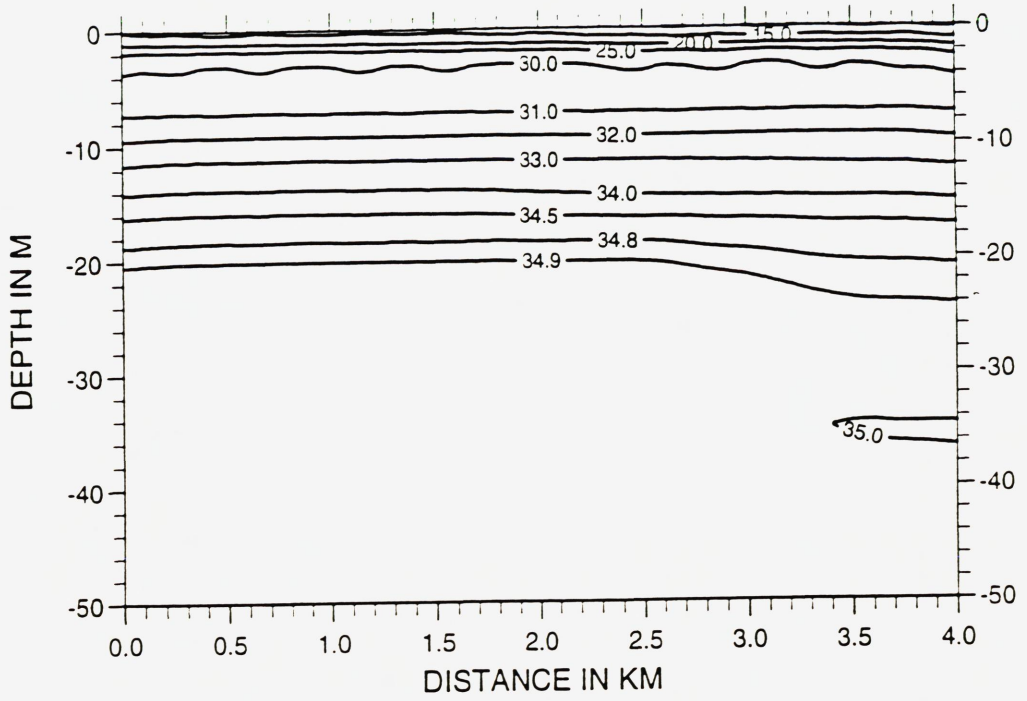

Figure 6b.

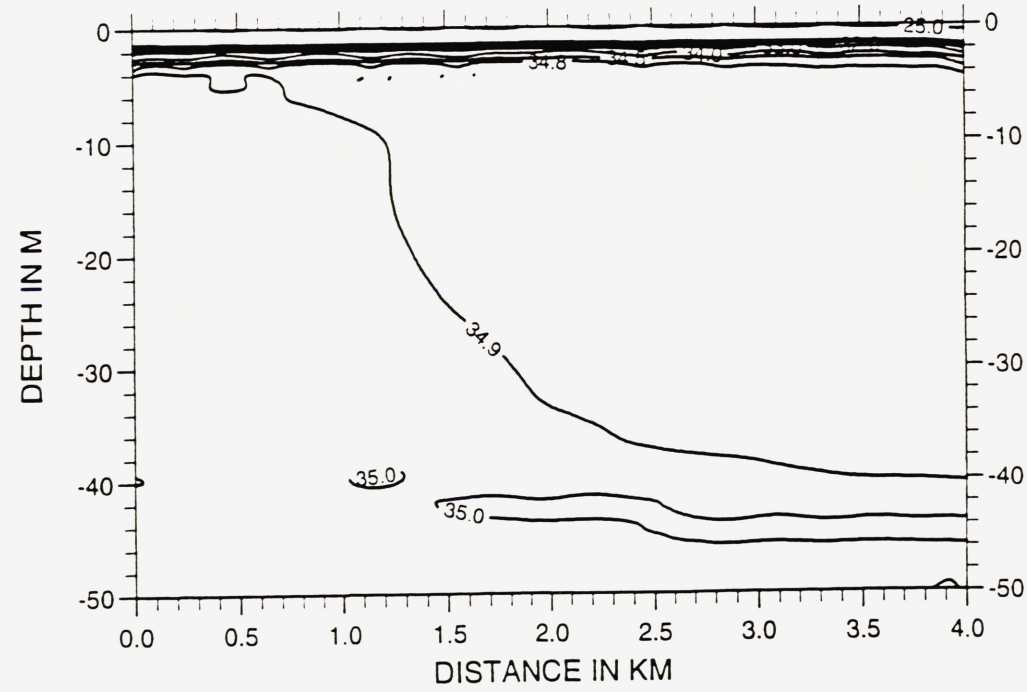

Figure 6. Cross fjord salinities in the upper 50m normal to a section at $x = 40000$m after 100 days. Figure 6a: Scenario b). Figure 6b: Scenario c).

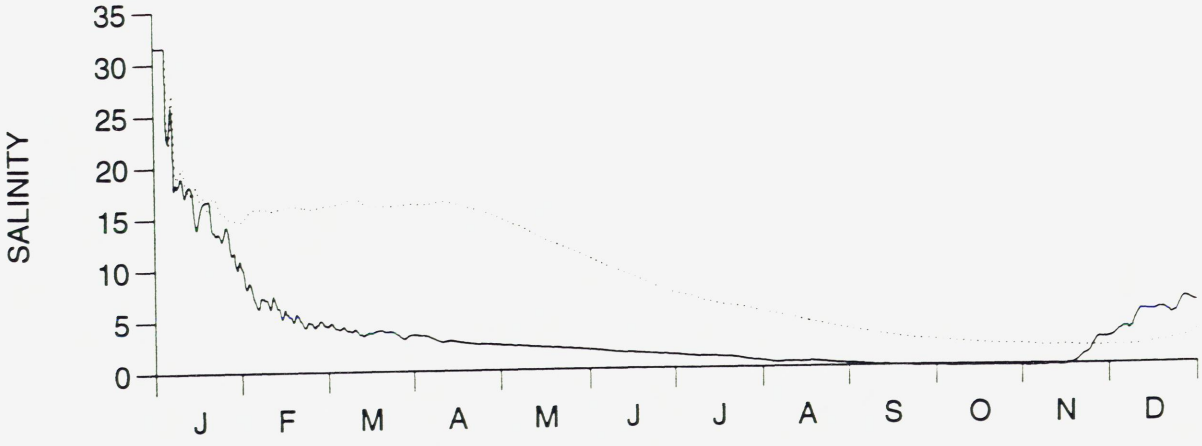

Figure 7. Salinities at $(x, y, z) = (30000\text{m}, 1000\text{m}, 0.5\text{m})$ for scenario b) (solid line) and scenario c) (dotted line).

5.2 Phytoplankton dynamics

Next we focus on the time and space evolution of the nutrient and phytoplankton fields. In figures 8a to 8e time series of average concentrations of inorganic nitrogen, phosphate, silicate, diatoms and flagellates are given. The averages are computed over the upper 30m of the inner 45000m of the fjord. The unit is mgm^{-3}. For phytoplankton the unit is $mgNm^{-3}$.

In figures 9 to 19 vertical along fjord sections at $y = 500$m of inorganic nitrogen, phosphate, silicate, diatoms and flagellates for the three cases are plotted. The unit is μM. We have chosen to give the nitrogen fields approximately at the same times as the maximum diatom and flagellate blooms. The diatom and flagellate fields are given at the time of the maximum bloom and then one field in the decaying period.

Figure 20 shows the total depth-integrated annual production per m^2 of the surface for scenarios b) and c). For scenario a) the production is 80 g C m^{-2} $year^{-1}$. The average production over the inner 45000m of the fjord is 88 g C m^{-2} $year^{-1}$ for scenario b) and 351 g C m^{-2} $year^{-1}$ for scenario c).

From the figures and integrated numbers one may conclude:

i) The most apparent result is the increased primary production for the submerged outlet case. The yearly primary production of the inner 45 km of the fjord is increased from approximately 80-90 g C m^{-2} $year^{-1}$ to 350 g C m^{-2} $year^{-1}$ by submerging 1/10 of our river to 50m depth. The horizontal distributions of the primary productions given in figures 20a and 20b, the time series 8d and 8e of average diatom and flagellate concentrations and the plots of vertical along fjord sections of diatoms and flagellates support this conclusion, see figures 14 to 19.

ii) There is a small increase in integrated primary production when going from the no river case to the river at the surface case. This is connected to the inflow of water in the 3 to 10 m layer below the surface outflowing layer. From figures 10a and 10b we note that the nutrients in this inflowing water are gradually depleted due to primary production, This is also supported by Figure 20a. The response on the phytoplankton on this inflow is also seen in figures 15a, 15b, 18a and 18b. The nutrient concentrations on inflow for our idealized cases are given in section 4 and especially for the surface they are questionable. For a real fjord the inflowing waters in the 3 to 10m layer may already be depleted in nutrients before entering the fjord in the productive part of the year and this will bring the yearly production for scenario b) to approximately the same level as for the no river case. On the other hand the inflow for the submerged case occurs below 40m which is also below the euphotic zone. Thus we are more confident that the nutrient concentrations of inflowing waters are of the correct order of size for this case. In the present studies we wanted to exclude possible primary production due to nutrients in the river water. Therefore, the added fresh water is chosen to be nutrient depleted.

iii) Even if there is a strong increase increase in primary production for scenario c) the production is still nutrient limited away from the submerged outlet in a large period of the summer. From the plots of vertical sections of nutrients, figures 11, 12 and 13, we note that 10-20 km away from the outlet the surface primary production may be nutrient limited. This means that with more rivers present along the fjord, there will be a potential for increasing the primary production even further.

iv) From figures 8d and 8e we note that the blooms for diatoms and flagellates starts at approximately the same times for the two first scenarios whereas the maximum blooms for the submerged case are substantially delayed. The signatures of these blooms on the nutrient concentrations are also clear in figures 8a to 8c. The delays in the start of the blooms for scenario c) may be explained by the dilution/mixing of all fields that occurs around and above the submerged outlet. Any maxima in plankton concentration will thus quickly be vertically diluted in this area and we must expect that this will slow down the growth rate. In addition the concentrations at peak production are much higher for scenario c) and it will therefore even with the same growth rate take some more time to build up the concentrations to their maxima.

v) From the plots of along fjord concentrations, for instance figures 16a, 16b, 19a and 19b, we note that we often find the maxima in diatom concentrations deeper than the maxima in flagellate concentrations. This is related to the sinking rates that are for high concentrations 12 times larger for diatoms than for flagellates, and also connected to diatoms higher affinity for light.

vi) In the plots of vertical sections of nutrients and plankton we find local maxima/minima in the concentrations, see for instance figures 11b, 11c, 11d, 12, 16a, 16b, 19a and 19b. These optima and the separation between them may be explained by the metabolic loss rates for phytoplankton and the velocity of the water masses. At $10°C$ the metabolic loss rates are $1.71 \times 10^{-6} s^{-1}$ which corresponds to a time scale of 6-7 days. Typical velocities of the water masses are $0.02 m s^{-1}$ which means that in 607 days the fields are transported approximately 12 km. This is in accordance with the modelled distances between maxima/minima.

Figure 8a.

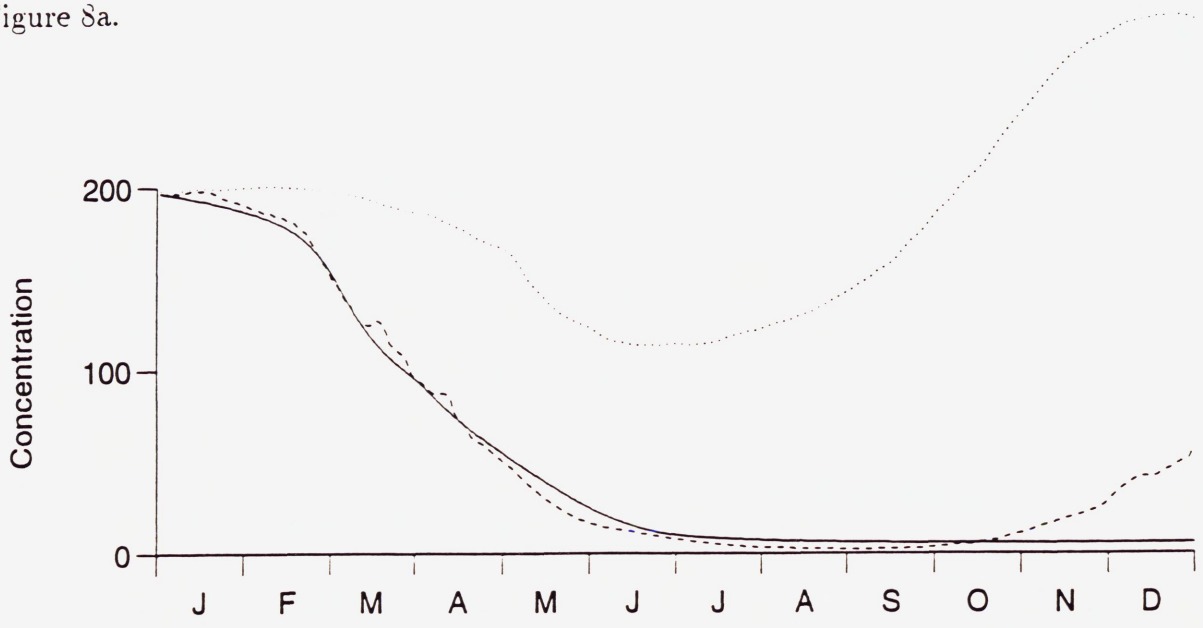

Figure 8b.

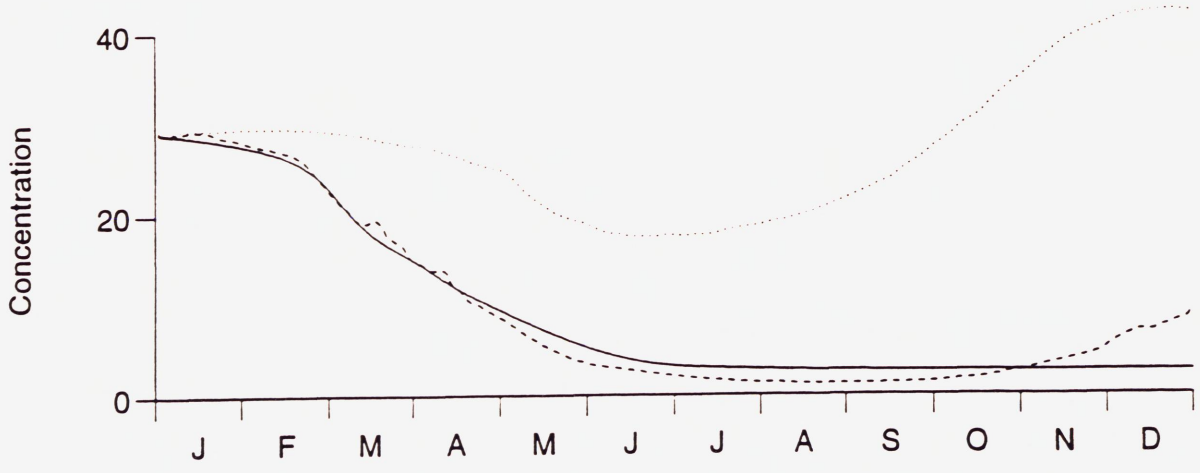

Figure 8c.

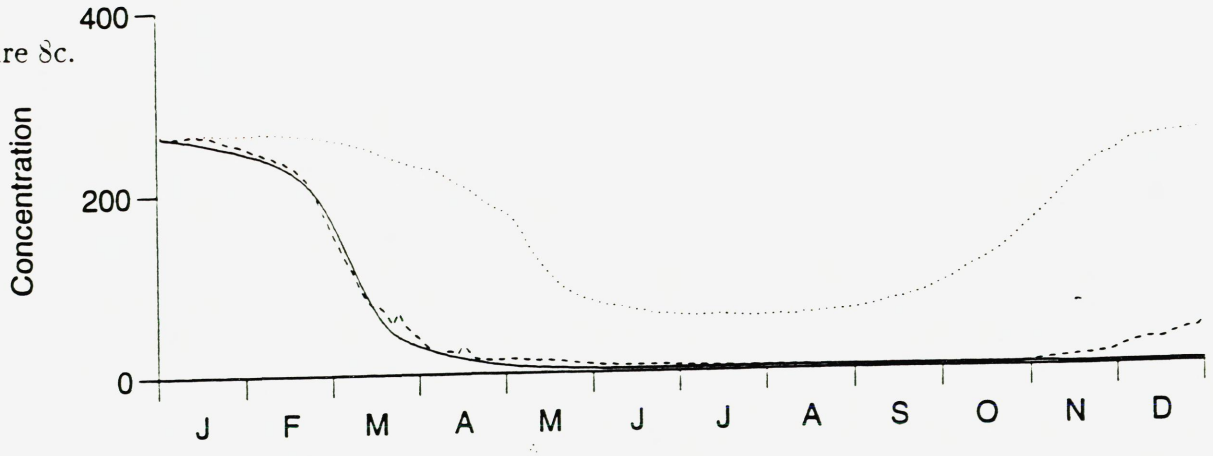

Figure 8d.

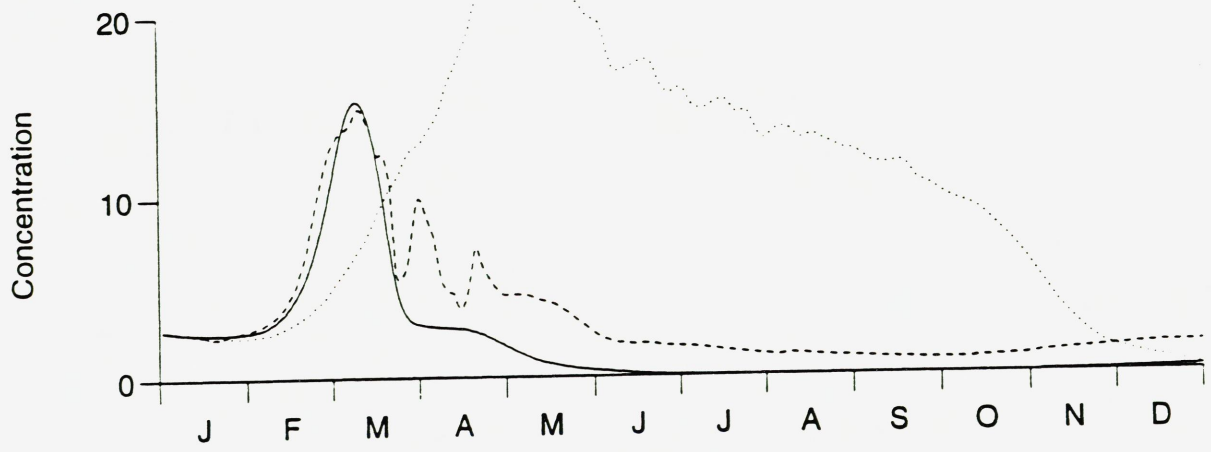

Figure 8e.

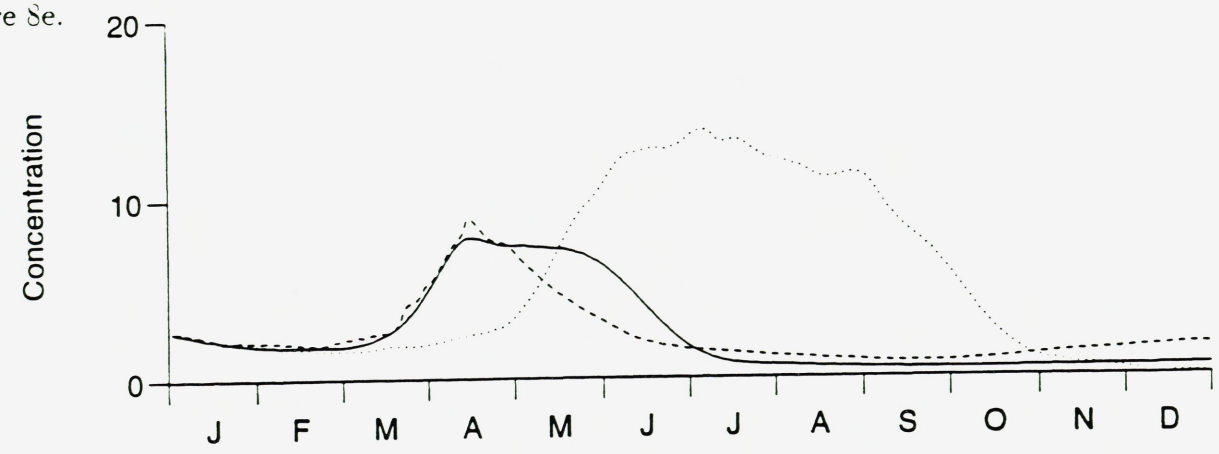

Figure 8. Time series of average concentrations of inorganic nitrogen (Figure 8a), inorganic phosphate (Figure 8b), inorganic silicate (Figure 8c), diatoms (Figure 8d) and flagellates (Figure 8e) in the upper 30m of the fjord for scenario a) (solid line), scenario b) (dashed line) and scenario c) (dotted line).

Figure 9a.

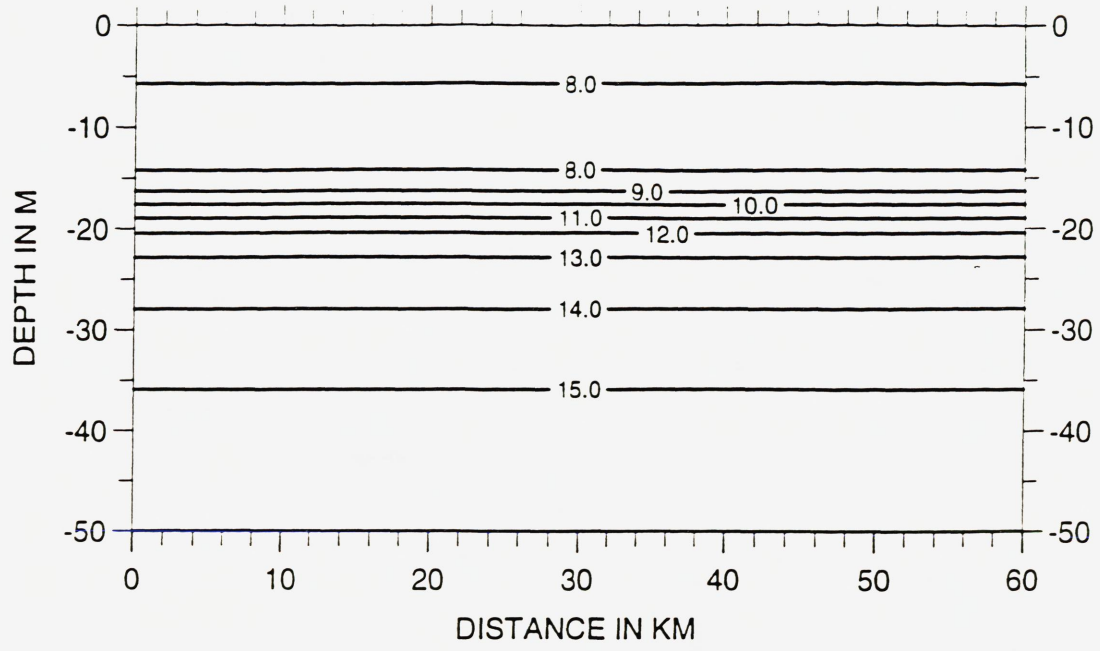

Figure 9b.

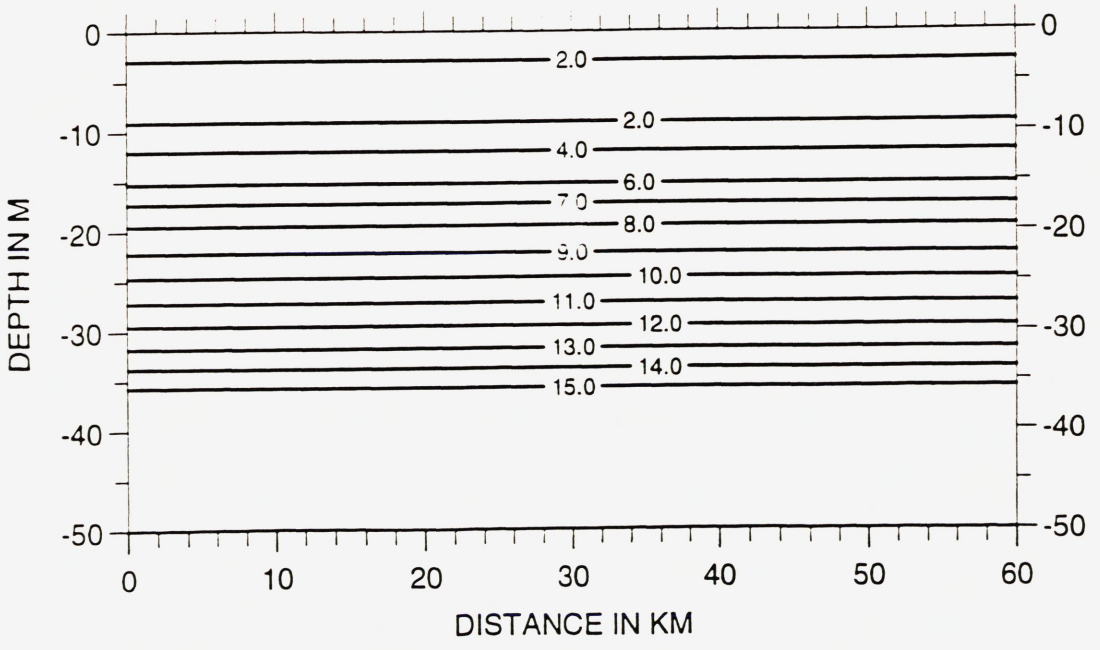

Figure 9. Along fjord section of the upper 50m of the fjord of inorganic nitrogen (μM) for scenario a) at y = 500m after 65 days (Figure 9a) and after 100 days (Figure 9b).

Figure 10a.

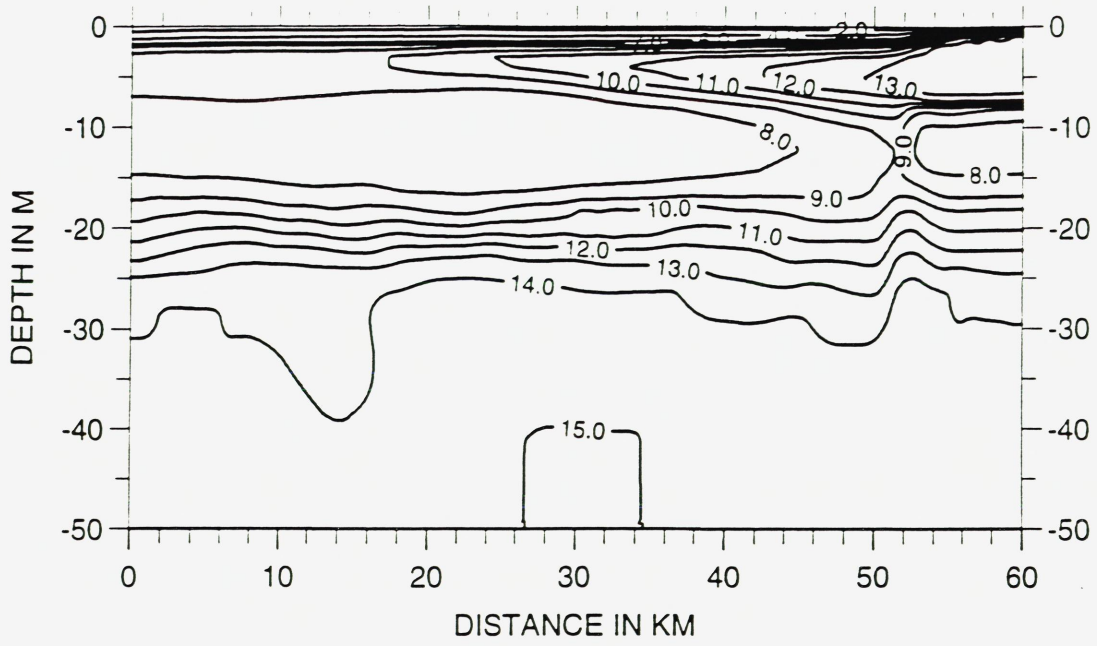

Figure 10b.

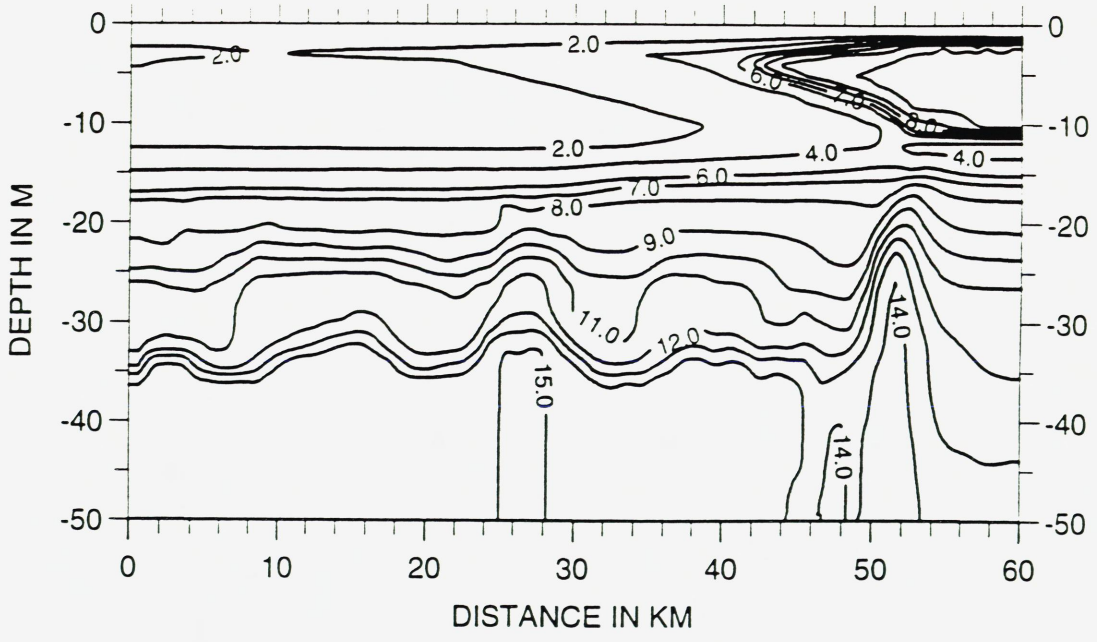

Figure 10. Along fjord section of the upper 50m of the fjord of inorganic nitrogen (μM) for scenario b) at y = 500m after 65 days (Figure 10a) and after 100 days (Figure 10b).

Figure 11a.

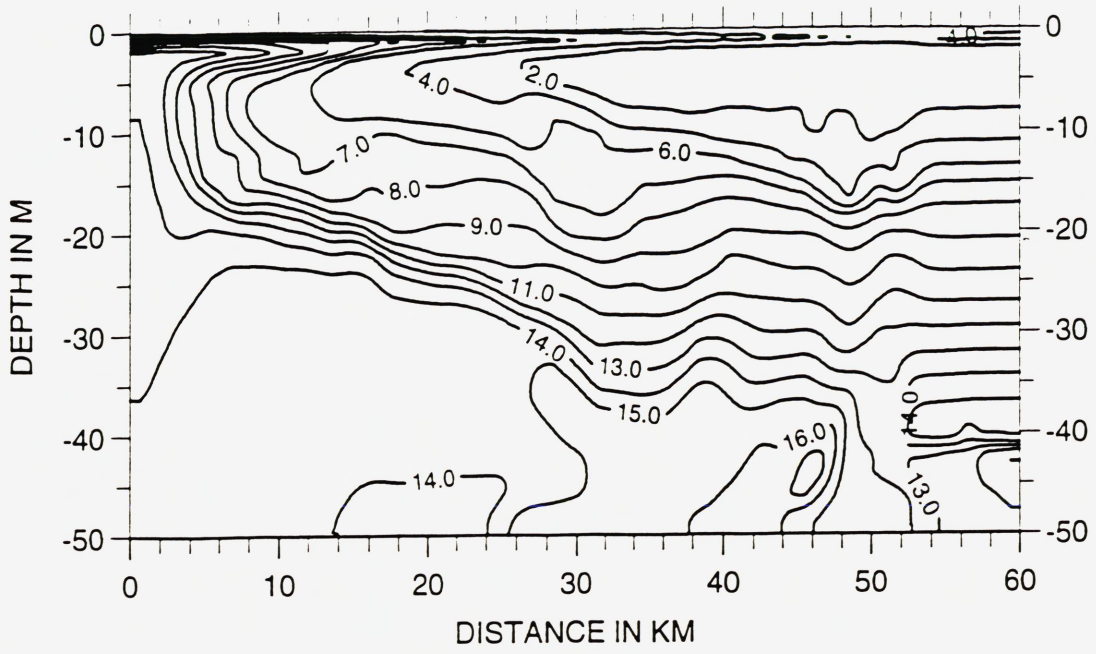

Figure 11b.

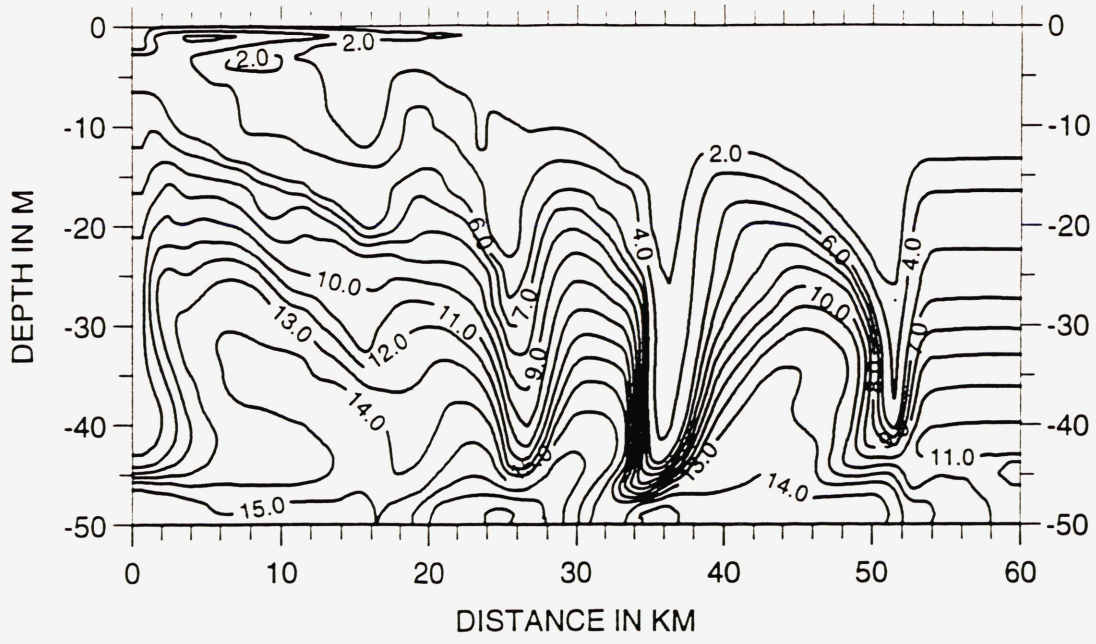

Figure 11c.

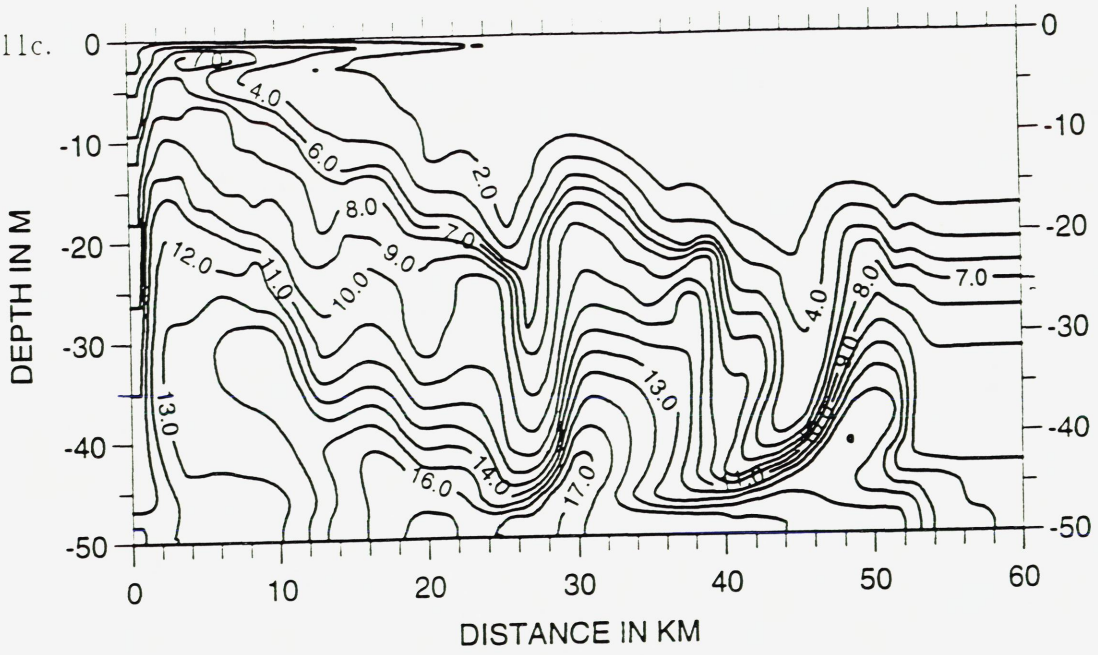

Figure 11d.

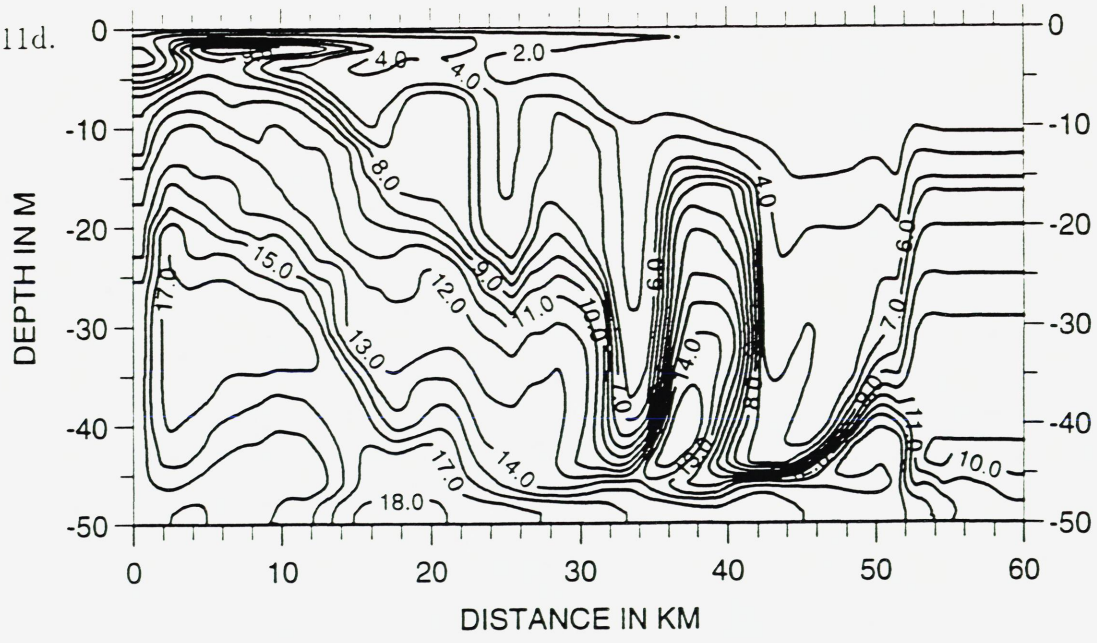

Figure 11. Along fjord section of the upper 50m of the fjord of inorganic nitrogen (μM) for scenario c) at $y = 500$m after 135 days (Figure 11a), after 185 days (Figure 11b), after 225 days (Figure 11c) and after 255 days (Figure 11d).

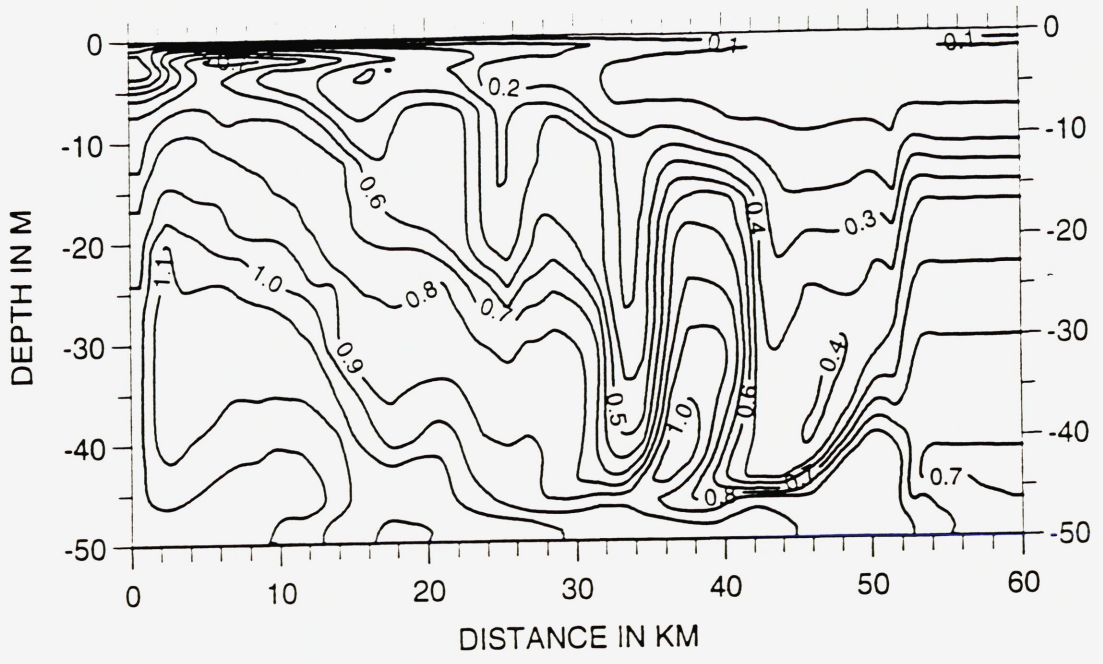

Figure 12. Along fjord section of the upper 50m of the fjord of inorganic phosphate (μM) for scenario c) at $y = 500$m after 255 days.

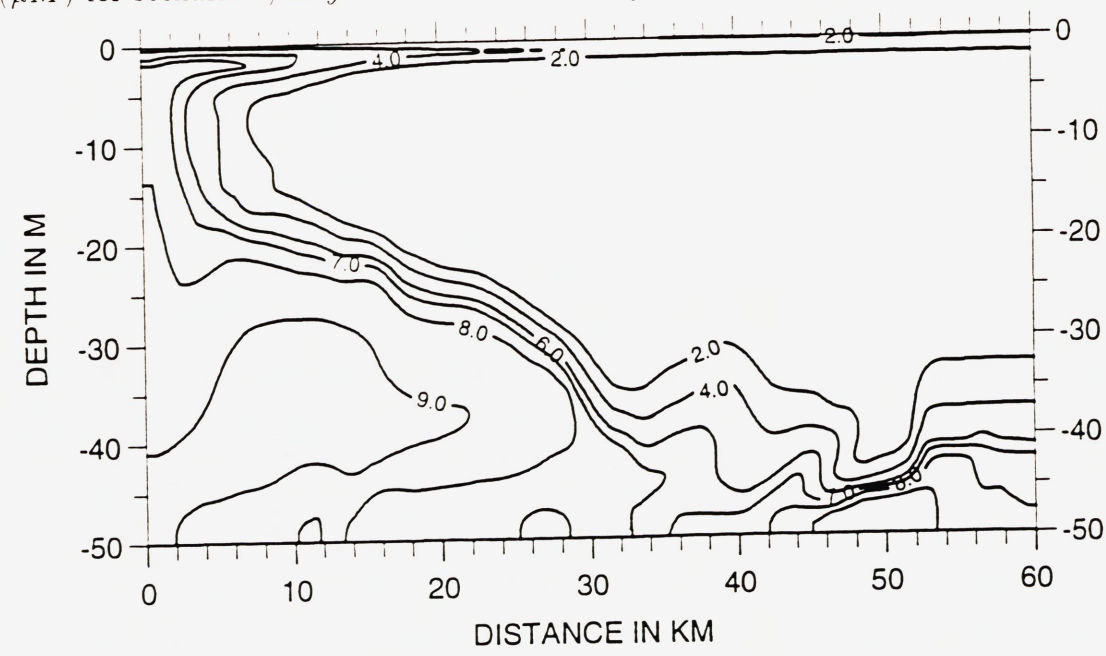

Figure 13. Along fjord section of the upper 50m of the fjord of inorganic silicate (μM) for scenario c) at $y = 500$m after 135 days.

Figure 14a.

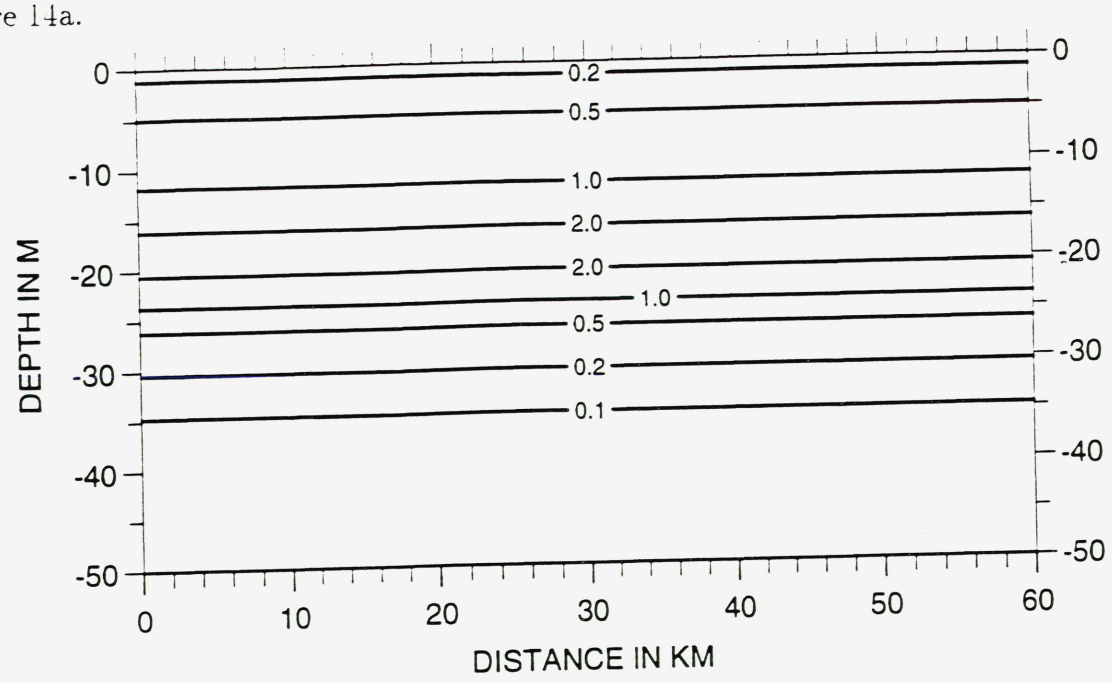

Figure 14b.

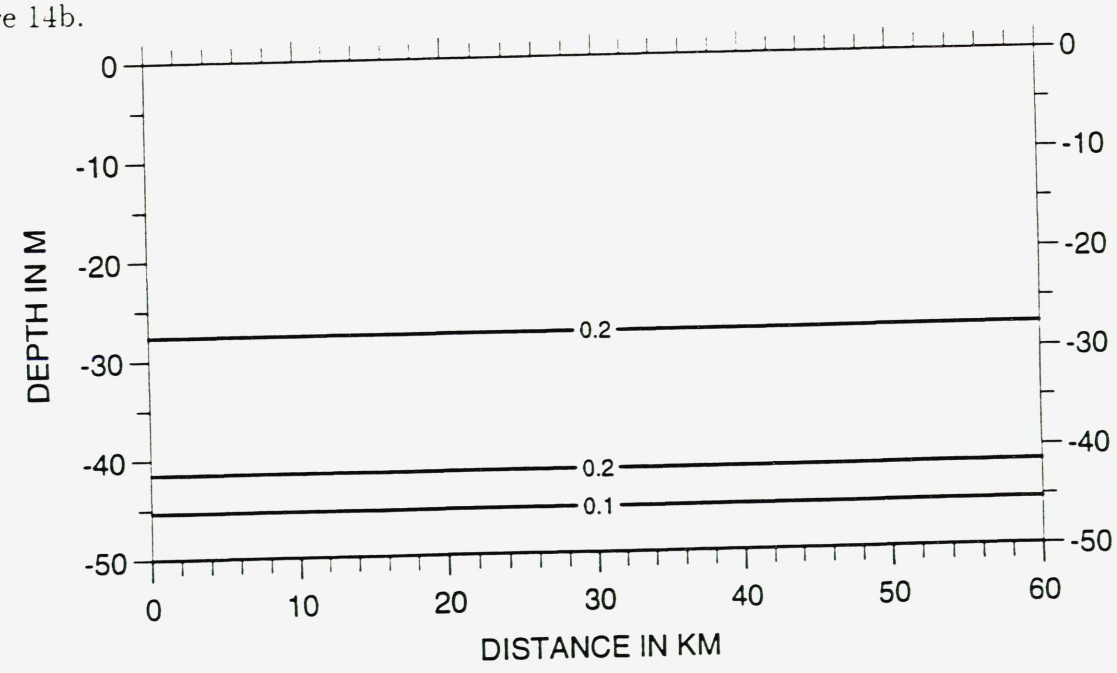

Figure 14. Along fjord section of the upper 50m of the fjord of diatoms (μM N) for scenario a) at y = 500m after 65 days (Figure 14a) and after 100 days (Figure 14b).

Figure 15a.

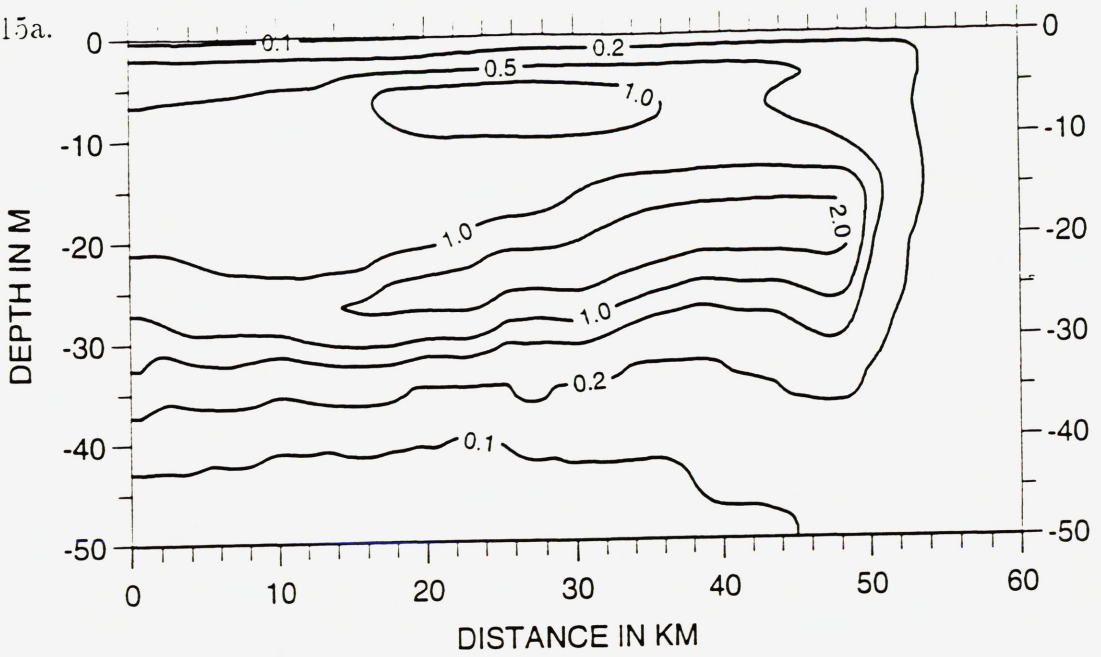

Figure 15b.

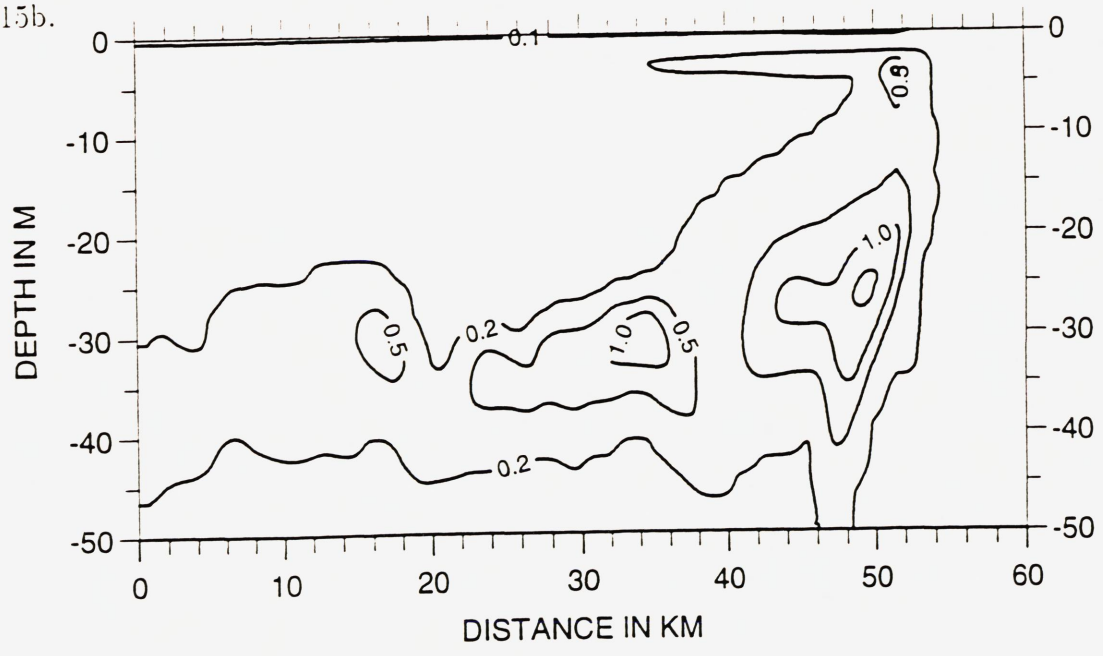

Figure 15. Along fjord section of the upper 50m of the fjord of diatoms (μM N) for scenario b) at y = 500m after 65 days (Figure 15a) and after 100 days (Figure 15b).

Figure 16a.

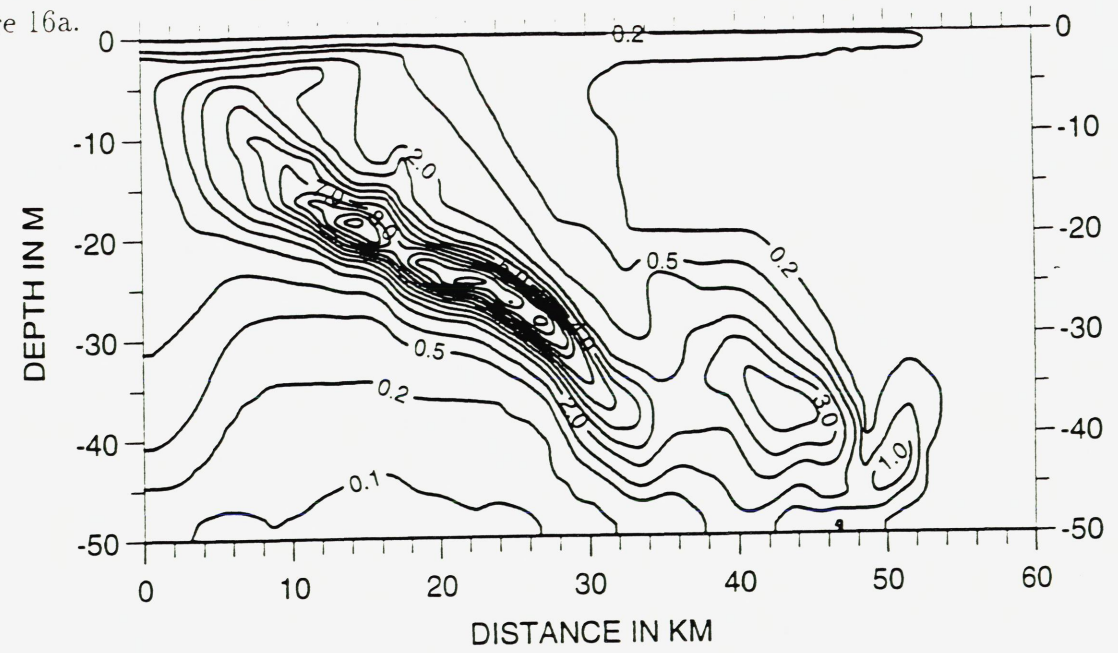

Figure 16b.

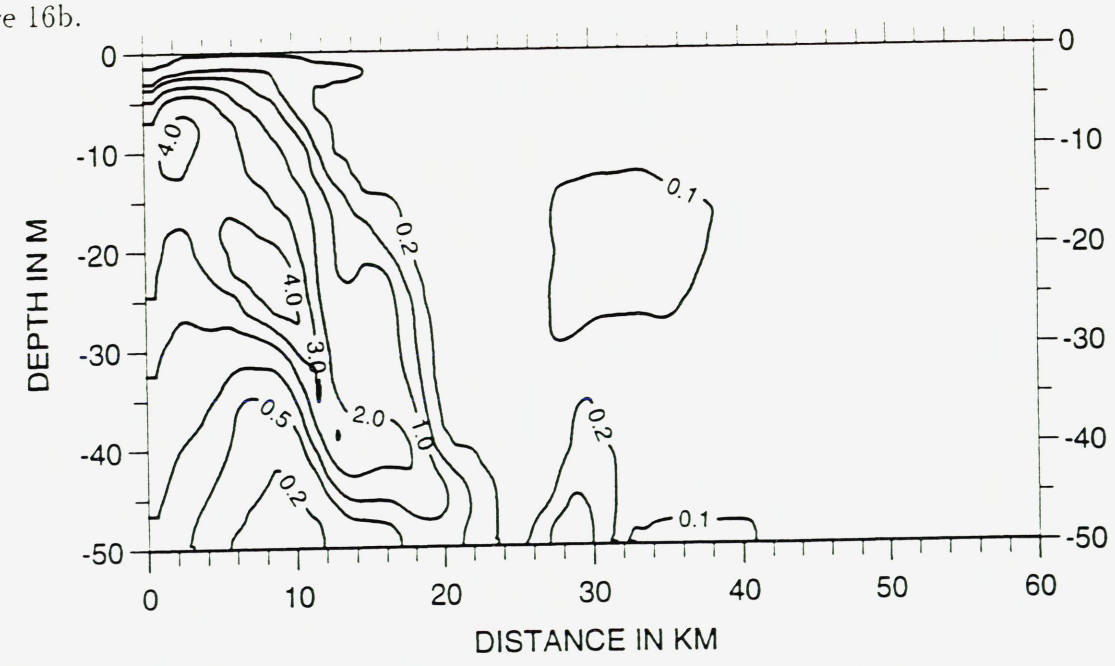

Figure 16. Along fjord section of the upper 50m of the fjord of diatoms ($\mu M\ N$) for scenario c) at $y = 500$m after 135 days (Figure 16a) and after 225 days (Figure 16b).

Figure 17a.

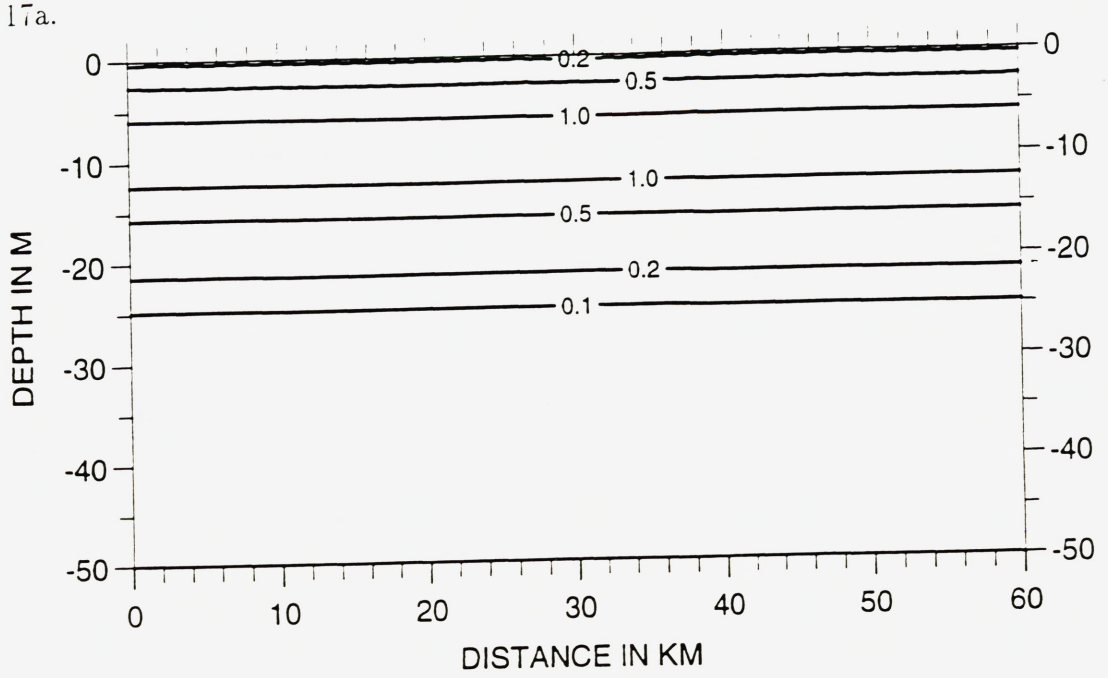

Figure 17b.

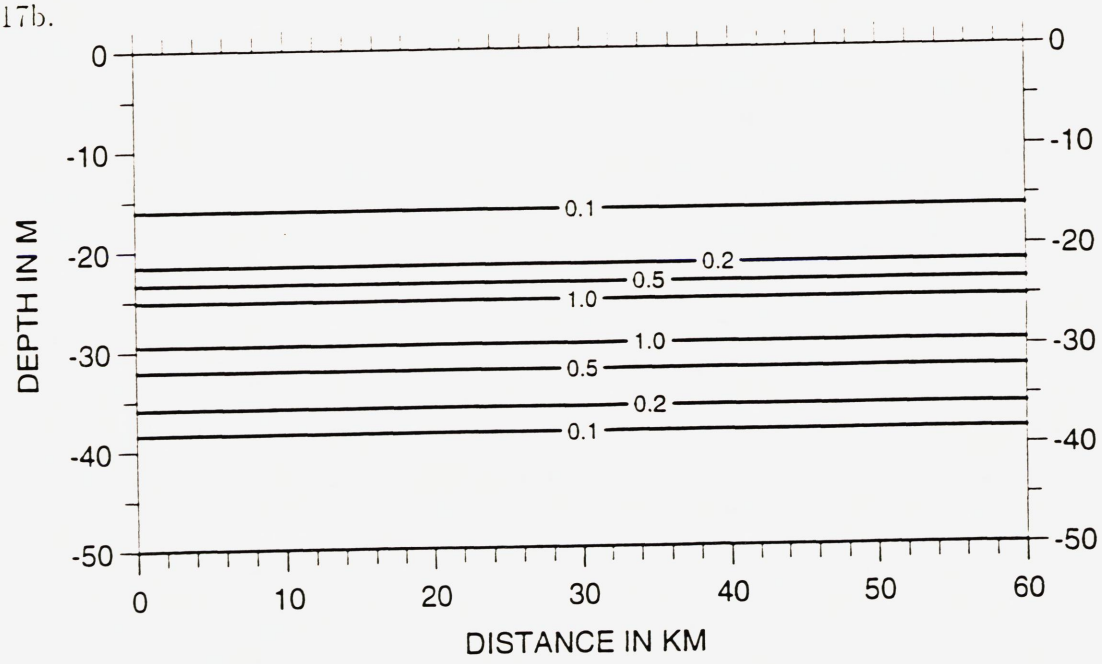

Figure 17. Along fjord section of the upper 50m of the fjord of flagellates (μM N) for scenario a) at $y = 500$m after 100 days (Figure 17a) and after 165 days (Figure 17b).

Figure 18a.

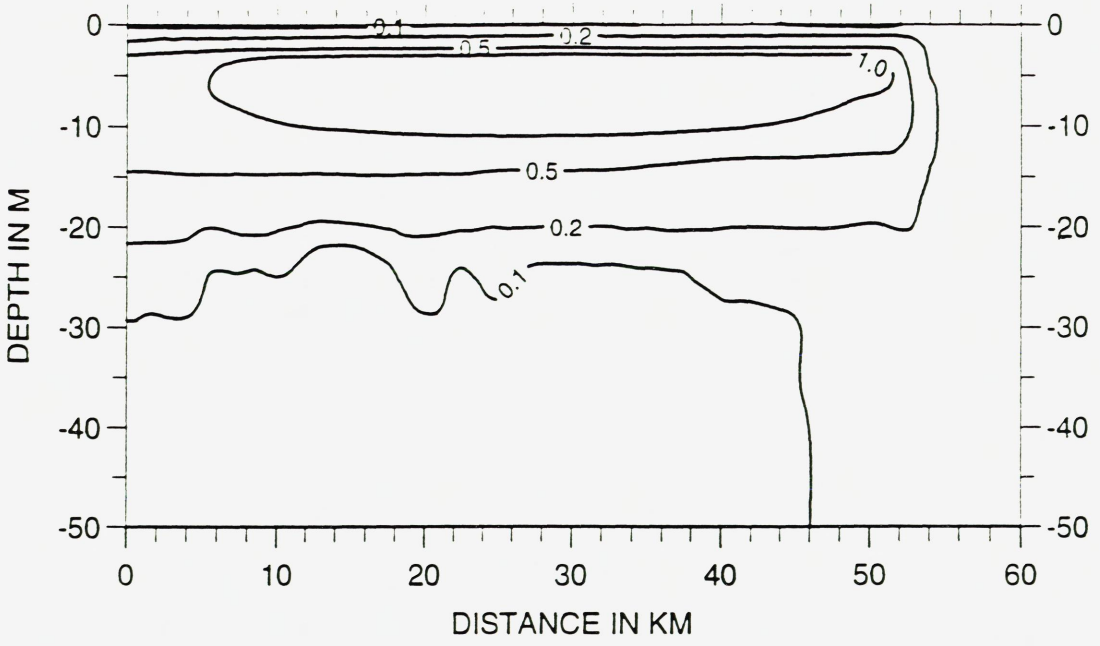

Figure 18b.

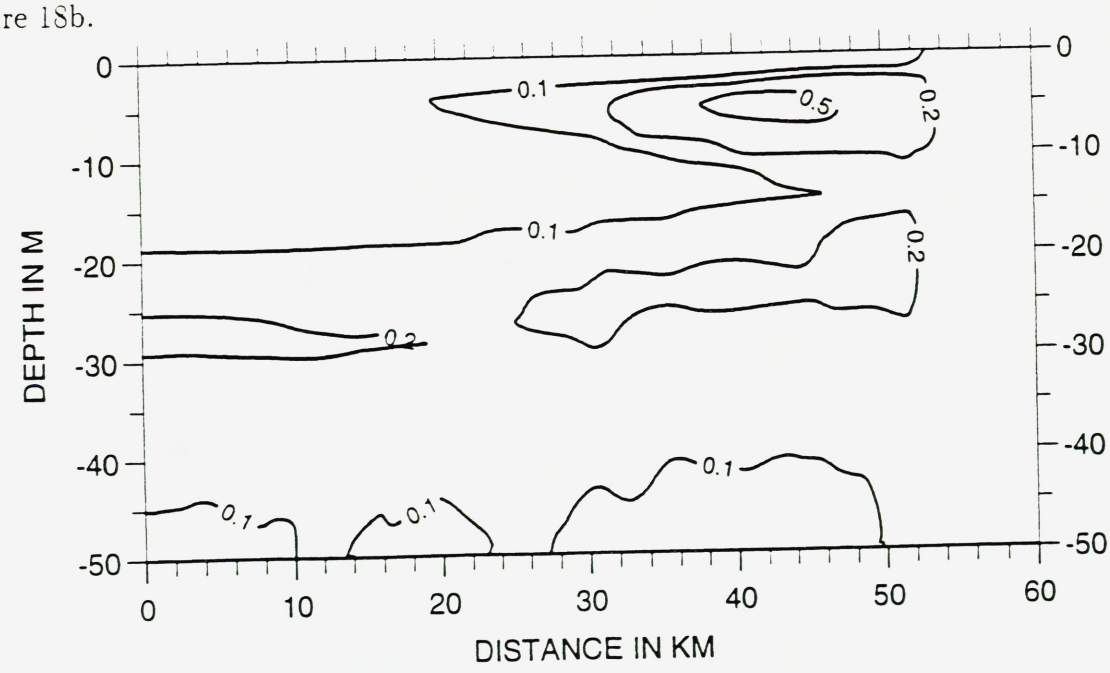

Figure 18. Along fjord section of the upper 50m of the fjord of flagellates ($\mu M\ N$) for scenario b) at $y = 500$m after 100 days (Figure 18a) and after 165 days (Figure 18b).

Figure 19a.

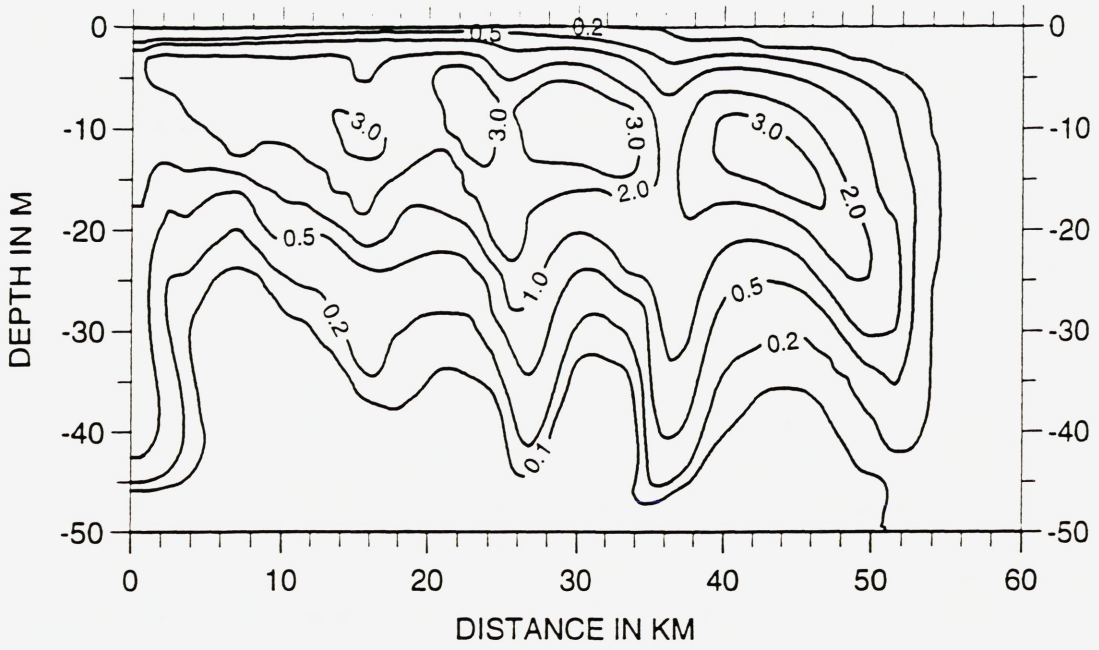

Figure 19b.

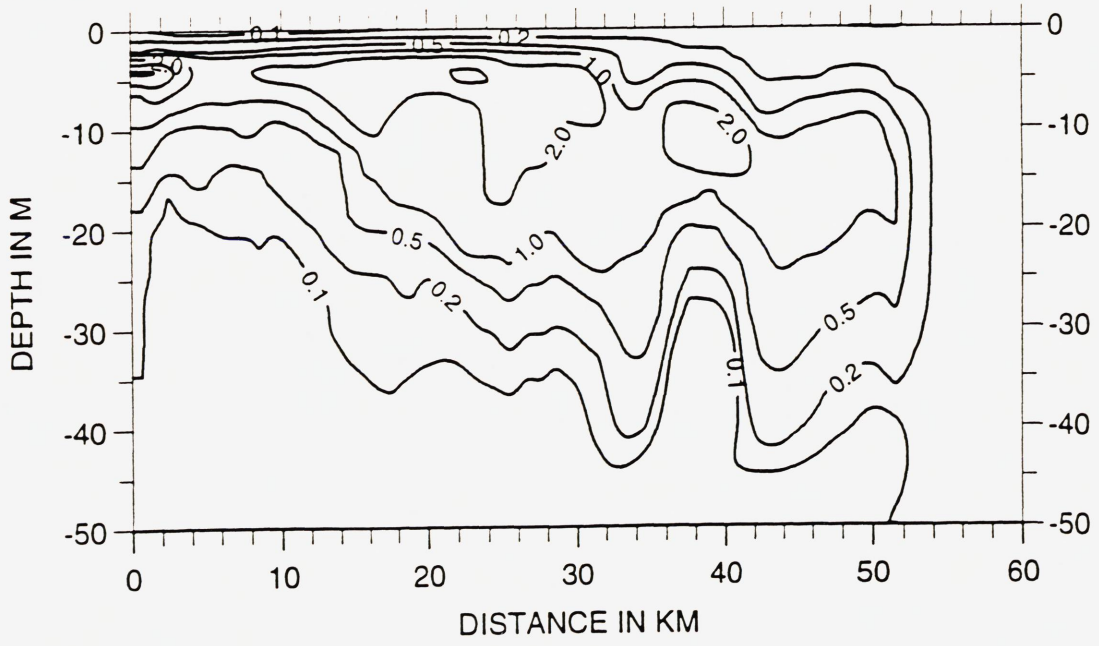

Figure 19. Along fjord section of the upper 50m of the fjord of flagellates (μM N) for scenario c) at $y = 500$m after 185 days (Figure 19a) and after 255 days (Figure 19b).

Figure 20a.

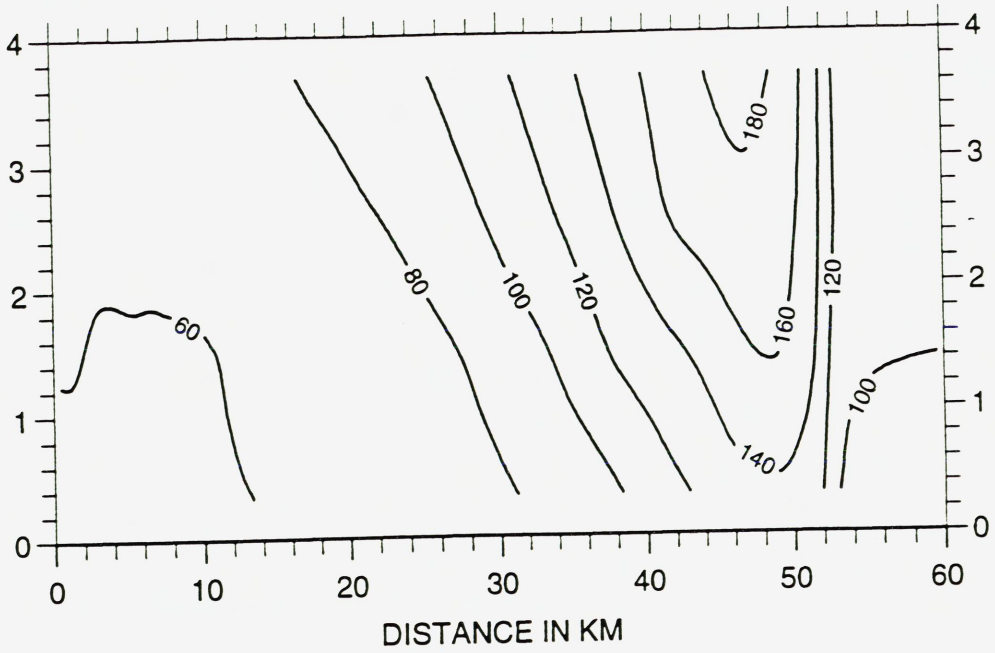

Figure 20b.

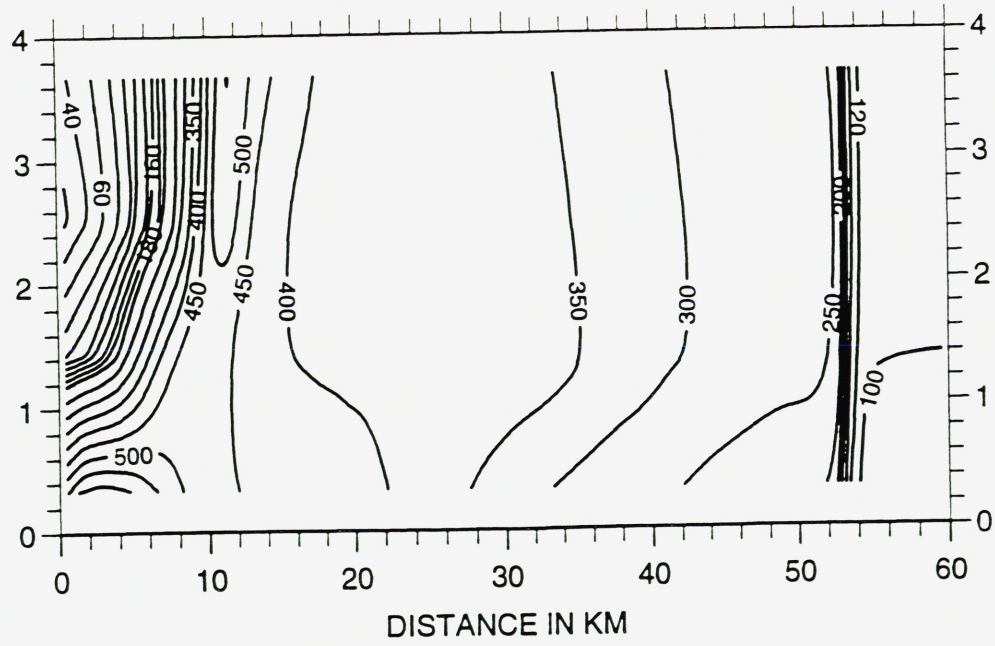

Figure 20. Modelled annual depth-integrated primary production in g C m^{-2} $year^{-1}$ for scenario b) (Figure 20a) and scenario c) (Figure 20b).

6 Discussion

The main conclusion from our simplified idealized fjord study is that there is a considerable potential for increased primary production in fjords and coastal areas by utilizing the volume and potential energy of freshwater to create upwelling of nutrient rich deeper water masses. We are aware that for real fjords both the forcing and the topography will be much more complex and the model should be run with more realistic forcing and topography before we make statements on the potential for increased primary production for a specific fjord. The results for a real fjord will, however, be affected by a number of processes acting more or less simultaneously and this will make it much more difficult to identify the sources of different effects.

By starting with fairly simple cases and then gradually increase the complexity, it will be more feasible to identify the effects of different kinds of forcing, topography and changes in the model specifics. Questions that we want answers to include:

a) The integrated primary production over the fjord may be regarded as a function of the submerged fresh water flux. Primary production = F(Fresh water flux). Will F be a linear function?

b) Will it be possible to utilize the available fresh water better if the submerged outlets are distributed throughout the fjord?

c) What will the effects of including wind with different velocities and directions be?

d) How will one or more components of the tide affect our result?

e) In the present study the added fresh water is nutrient depleted. How will our results be affected if the added fresh water is allowed to have more realistic concentrations of nutrients?

f) When we start to introduce fresh water into an undisturbed system, there will be a transient phase with much kinetic energ and vertical mixing. Is it possible to utilize the fresh water better for primary production by releasing it in pulses to the fjord in stead of as a steady flow?

g) In the present study the outlet is submerged to 50m depth. How is the functional relationship between integrated primary production and release depth?

h) The present study is done for a flat bottom fjord. In most Norwegian fjords there are sills at the mouth of the fjords. To what extent will the results be affected by introducing sills of different heights into the fjord?

i) To what extent will the results be affected by introducing one or more narrowings into the fjord?

j) The fjord model system should be connected in a more realistic way to a model

system for the coast. What will the effects be of extending our model domain to include some part of the coast?

k) In the present model runs the horizontal grid spacing is 1km and thus we have ignored small scale effects that at least in the nearfield of the outlets will be important. How will a study with better horizontal resolution, with a focus on the nearfield of the outlet, affect our conclusions?

l) In the present study the hydrostatic assumption has been used in the physical model. This means that the vertical velocities are assumed to be much smaller than the horizontal components. This is obviously wrong near and above the submerged fresh water outlet. The question is: 'Will our main conclusions be affected if we run the experiments with a non-hydrostatic model?'

m) The vertical exchange processes are essential for such studies and we have used Richardson number formulations to compute the vertical eddy viscosities/diffusivities K_M and K_H. For unstable water masses, we have selected $K_M = K_H = 0.05m^2s^{-1}$ which give an intensive mixing. To what extent will the model results depend on the choices of parametrizations of vertical exchange processes?

n) The quality of the model results are clearly dependent of the chosen boundary values and boundary conditions. Are there better choices of OBCs and boundary values that may improve the quality of the model results?

Ideally we could hope that the answer to one of these questions would be independent of the other choices made of forcing, topography and model specifics. This will certainly not be the case so also experiments where we vary more than one parameter will be of interest. With for instance 5 possible cases to study for each of the above questions, we end up with $5^{14} \sim 6 \times 10^9$ possibly interesting combinations indicating that as a first approach it will nevertheless be wise to focus on variation of one parameter at the time.

Acknowledgement. The numerical experiments have been run on a Cray ORIGIN 2000 installed at Parallab, University of Bergen, and we thank Parallab for allowing access to the machine and kind support.

References

[1] D.L. Aksnes and J.K. Egge. A theoretical model for nutrient uptake in phytoplankton. *Marine Ecology Progress Series*, 70:65–72, 1991.

[2] D.L. Aksnes, K.B. Ulvestad, B.M. Balino, J. Berntsen, J.K. Egge, and E. Svendsen. Ecological modelling in coastal waters: Towards predictive physical-chemical-biological simulation models. *OPHELIA*, 41:5–36, 1995.

[3] ANON. MARICULT- Programme description, Hydro Research Centre, Porsgrunn, Norway, 1994.

[4] J. Berntsen, D.W. Skagen, and E. Svendsen. Modelling the transport of particles in the North Sea with reference to sandeel larvae. *Fisheries Oceanography*, 3:81–91, 1994.

[5] J. Berntsen, M.D. Skogen, and T.O. Espelid. Description of a σ-coordinate ocean model. Technical Report Fisken og Havet Nr. 12, Institute of Marine Research, 1996.

[6] J. Berntsen, E. Svendsen, and M. Ostrowski. Validation and sensitivity study of a sigma-coordinate ocean model using the Skagex dataset, 1996. ICES CM 1996/C:5.

[7] M.D Cox and K. Bryan. A numerical model of the ventilated thermocline. *J. Phys. Oceanogr.*, 14:674–687, 1984.

[8] R.W. Eppley. Temperature and phytoplankton growth in the sea. *Fishery Bulletin*, 70:1065–1085, 1972.

[9] A. Foldvik. Personal communication, 1996.

[10] E.A. Martinsen and H. Engedahl. Implementation and testing of a lateral boundary scheme as an open boundary condition in a barotropic ocean model. *Coastal Engineering*, 11:603–627, 1987.

[11] W.H. Munk and E.R. Anderson. Notes on a theory of the thermocline. *J.Marine Res.*, 7:276–295, 1948.

[12] T. Platt and A.D. Jassby. The relationship between photosynthesis and light for natural assemblage of coastal marine phytoplankton. *J. of Phycology*, 12:421–430, 1976.

[13] A. Skartveit and J.A. Olseth. Modelling slope irradiance at high latitudes. *Solar Energy*, 36:333–344, 1986.

[14] A. Skartveit and J.A. Olseth. Varighetstabellar for timevis belysning mot 5 flater på 16 norske stasjonar(in norwegian). Technical Report Rapport 7-1988, Geophysical Institute, Meteorological Division, Allegt. 70, N-5007 Bergen, Norway, 1988.

[15] M.D. Skogen. A user's Guide to NORWECOM. The NORWegian ECOlogical Model system. Technical Report 6, Institute of Marine Research, 1993.

[16] M.D. Skogen, E. Svendsen, J. Berntsen, D. Aksnes, and K. Ulvestad. Modelling the Primary Production in the North Sea using a coupled Three-dimensional Physical- Chemical-Biological Ocean Model. *Estuarine, Coastal and Shelf Science*, 41:545–565, 1995.

[17] M.D. Skogen, E. Svendsen, and M. Ostrowski. Quantifying volume and nutrient transports and primary production with the Norwegian Ecological Model System (NORWECOM), 1995. Submitted.

[18] UNESCO, 1981. Tenth report of the joint panel on oceanographic tables and standards. UNESCO Technical Papers in Marine Sci. No. 36. UNESCO, Paris.

[19] D.-P. Wang. Mutual intrusion of a gravity current and density front formation. *J. Phys. Oceanogr.*, 14:1191–1199, 1984.